THE UNIVERSITY OF ALBERTA

AN APPLICATION OF THE P-CODA SPECTRAL RATIO METHOD TO CRUSTAL STRUCTURE IN CENTRAL ALBERTA

by

© KENNETH F. SPRENKE

A THESIS

SUBMITTED TO THE FACULTY OF GRADUATE STUDIES AND RESEARCH

IN PARTIAL FULFILLMENT OF THE REQUIREMENTS FOR THE DEGREE

OF MASTER OF SCIENCE

DEPARTMENT OF PHYSICS

EDMONTON, ALBERTA

SPRING, 1972

THE UNIVERSITY OF ALBERTA

FACULTY OF GRADUATE STUDIES AND RESEARCH

The undersigned certify that they have read, and recommend to the Faculty of Graduate Studies and Research, for acceptance, a thesis entitled AN APPLICATION OF THE P-CODA SPECTRAL RATIO METHOD TO CRUSTAL STRUCTURE IN CENTRAL ALBERTA submitted by Kenneth F. Sprenke in partial fulfillment of the requirements for the degree of Master of Science.

ABSTRACT

The P-codas of four Aleutian teleseismic events, recorded by an array of three portable seismic stations near Leduc, Alberta, have been analyzed by the spectral ratio method for purposes of determining the reliability of this method and of obtaining information about crustal structure.

The general characteristics of the spectral ratios were found to be reasonably consistent at each of the stations in 0.5 to 3.0 Hz range. However, a considerable difference was noted in the spectral ratios from station to station, a rather surprising result since the stations were only about ten kilometers apart in a presumably uncomplicated geological region consisting of practically horizontal sedimentary layering.

Many theoretical spectral ratios were generated using crustal models based on known geology along with varied assumptions about unknown crustal parameters. While no exact match has been found at this time between theoretical and observed spectral ratios, it is possible that the upper crust in the Leduc area is typified by 1) a very low S-wave velocity in the surficial layers, 2) a Poisson's ratio of one-third in the softer sedimentary layers, and 3) a low velocity layer of thickness approximately 3.5 kilometers in the basement immediately beneath the sediments.

The effect on the P-coda spectral ratio of anisotropy in the sedimentary layers was studied using a modified version of the Haskell-Thompson matrix method adapted to transversely isotropic

media for the case of body waves by E.R. Kanasewich. Anisotropy was found to have a considerable effect on the spectral ratios at high angles of incidence, but almost no effect for low angles of incidence. For the Aleutian events in this study, sedimentary anisotropy was not found to have an important effect on the spectral ratios.

ACKNOWLEDGEMENTS

I wish to thank sincerely Dr. E.R. Kanasewich for his guidance and advice during the course of this study.

I would also like to acknowledge the help of Mr. Dave Malinsky, Mr. Charles McCloughan, and Mr. Jim Montalbetti who maintained the field equipment and pre-processed the field data during the fall of 1969.

The writer was partially supported by a National Research Council bursary and by a University of Alberta Graduate Teaching Assistantship during this research.

TABLE OF CONTENTS

LIST OF ILLUSTRATIONS

CHAPTER 1

THE SPECTRAL RATIO METHOD OF DETERMINING CRUSTAL STRUCTURE

1.1 Introduction

In the past decade, there have been several attempts by various researchers to use the spectral characteristics of the P-wave together with the Haskell-Thompson matrix formulation for the solution of the elastic wave equation to determine the nature of the crust. This is an indirect inverse problem in that it involves the generation of many crustal models in hopes of finding a best fit to observed data and like most inverse problems in geophysics, the solution is not necessarily unique. Furthermore, the observed data itself has been found to be quite susceptible to noise from sources other than those included in the Haskell-Thompson theory. Because of these problems, the degree to which the Haskell-Thompson formulation is capable of resolving the crustal structure still remains undetermined. The purpose of this thesis is to find to what extent the application of the Haskell-Thompson matrix to crustal structure is possible and, then, to actually apply the method to determine the crustal structure as accurately as possible in central Alberta.

When the crust of the earth is penetrated by seismic waves, its frequency response to the signal depends on the elastic parameters and thicknesses of the rock layers within the crust. If the crust is assumed to be composed of strictly horizontal layers, a condition generally verified by refraction, surface wave and teleseismic travel time studies, the frequency response or transfer function of the earth to plane P or S waves can be computed by solving the wave equation using

the continuity of stresses and particle displacements at each interface and the vanishing of stresses at the free surface as boundary conditions. The Haskell-Thompson matrix formulation performs this calculation for any number of horizontal layers in terms of a 4 x 4 matrix whose members are a function of the parameter of each layer and the angle of incidence of the source of excitation.

The crust acts like a linear filter on incoming seismic waves and its effect on resultant seismograms is quite significant and has been observed at seismological stations for many years. Gutenberg (1934) found that certain seismic stations showed a tendency to detect seismic waves of a given period. Neumann (1954) noticed that stations located on deep sedimentary rocks recorded less amplitude for a given earthquake than those stations located directly on the granite basement. The effect of the upper crust on the amplitudes of body waves led Gutenberg and Richter (1936) to devise station correction factors for earthquake magnitude determinations.

It has been only recently, however, that attempts have been made to invert the observed crustal effects on seismic body waves and, hence, arrive at the crustal structure. Such a method would be quite valuable to crustal studies in that the only other ways to detail the structure of the crust, namely, refraction and reflection seismology, are plagued with the necessity of artificial sources, extensive field operations, and accurate time correlations between stations. An inversion method, however, based on the application of the Haskell-Thompson matrix formulation to earthquake body waves would be free from the above mentioned encumberances and would, thus, be a very inexpensive method of obtaining crustal information. Phinney (1964) was the first to use

the method when he compared the ratio of long period spectra of vertical and horizontal P-codas of large earthquakes with the ratio of vertical and horizontal transfer functions as calculated by the Haskell-Thompson matrix formulation. His results for such long periods (up to 0.2 Hz) were quite reasonable. Fernandez (1966) also obtained good fits between observed and calculated spectral ratios in the same frequency range for simple 2-layer models (one layer and half space). He noted that any estimation of different layers within the crust was neither "precise nor unique" and suggested that spectra of shorter period records would give much more detailed information about the structure within the crust. Ellis and Basham (1968) attempted the inversion for shorter period (0.1 to 3.0 Hz) data in the central Alberta plains where the crustal structure was presumably well known but obtained disappointing agreement between the theoretical and observed spectra. Alpaslan (1968) also used short period data in such an inversion process but without much success. Hasegawa (1971) obtained fairly promising results for the method at both long and short period results over a relatively simple crust at Yellowknife, N.W.T.

The University of Alberta, at the present time, has in operation nine portable broad band seismic systems capable of recording both long and short period earthquake waves simultaneously. It is anticipated that this system will be useful in determining the actual limitations and possibilities in inverting P-wave spectral data.

1.2 The Inversion of the Spectral Ratio

A signal transmitted through the crustal layers of the earth and recorded at the surface is modified in a manner depending on the

density and elastic properties of the media. Such a recorded signal is expressible in the time domain as the convolution of the source function with the crustal transfer function. That is,

$$\text{Recorded Seismograms } (t) = \text{Source } (t) * \text{Transfer Function } (t) \qquad 1.1$$

where * indicates a convolution process and t represents time. It is far more convenient to consider the above relation in the frequency domain for several reasons: 1) it is easy to calculate the crustal transfer as a function of frequency using normal mode theory via the Haskell-Thompson matrix formulation, 2) statistical methods of reducing recorded ground motion to its spectral components are readily available, and 3) convolution in the time domain becomes simple multiplication in the frequency domain. In the frequency domain, therefore:

$$\text{Spectrum of recorded data} = \text{Source} \cdot \text{Crustal Transfer Function} \qquad 1.2$$

It should be noted that the term spectrum includes both phase and amplitude information as a function of frequency, hence, the crustal transfer function itself is a complex quantity for each frequency.

If one is considering only plane P-waves as the source, all of which are incident on the base of the crust at the same angle, then the resultant motion on the surface will be only in the plane determined by the radial and vertical directions. Hence the recorded data can be specified in terms of two components only: the vertical and horizontal motion.

Since both the vertical and horizontal ground motion are due

to exactly the same source one can write:

$$Z(f) = \text{Source}(f) \cdot V(f)$$
$$H(f) = \text{Source}(f) \cdot R(f) \qquad 1.3$$

where: Z and H are the vertical and horizontal spectrums of the recorded data; V and R are the vertical and horizontal crustal transfer functions; and f represents frequency. Simple division of these two equations leads to the basis for the inversion of P-wave spectral data:

$$\frac{Z(f)}{H(f)} = \frac{V(f)}{R(f)} \qquad 1.4$$

that is, the ratio of the vertical to horizontal spectrums of the recorded seismograms is equal to the ratios of the vertical to horizontal transfer functions. The source function is, therefore, eliminated by the division process, and the observed spectral ratio can be matched to the theoretically calculated ratio of transfer functions for any assumed crustal model.

In practice, however, several difficulties arise. In regard to the eliminations of the source, one must recall the assumptions about it:

1) It must be a plane wave. From a geometric point of view this assumption should be quite valid for most teleseismic earthquakes; but any large lateral heterogeneities in the mantle below the crust could alter the plane characteristics of the wave, i.e. an active or relict subduction zone.

2) The source of plane waves impinging on the layered media must consist of pure compressional (or shear) motion. Because of the difference in P and S velocities, the distance between the source origin and the point of observation acts as a delay line to separate P and S motion. Standard travel time curves are, therefore, useful for determining how much of the recorded data at particular epicentral distance should be P motion. The real danger of S waves entering the P-coda comes not from shear waves generated near the source but rather from shear waves produced by P-S conversions in the mantle beneath the crust. While there is no seismic evidence of significant first order velocity jumps in the mantle, there are large velocity increases especially in the 100 to 700 KM depth range which might look like discontinuities to seismic waves of certain wavelengths.

3) All the components of the source wave must arrive at the base of the crust at the same angle of incidence. This assumption eliminates the use of relatively close events as sources since it is quite likely that P-waves recorded at the station have arrived by many different paths. Alpaslan (1968) attempted to use Project Early Rise explosion data to invert the P-wave spectral ratios, but did not have much success partly because of the varying angles of incidence of the incoming P-waves as they were refracted or reflected along different mantle boundaries. It is, therefore, important that the events chosen for analysis be at a safe distance from the recording station to avoid these multiple arrivals.

4) Another possible cause for the angle of incidence not being constant at the base of the crust for the entire P-coda is the possible presence of first order discontinuities in the mantle. Any

multiple reflection in the mantle will affect some frequencies more than others, and the angle of emergence of the source wave from the mantle which impinges on the crust would be a function of frequency, rather than a constant as is assumed in the theory. This effect can be reduced by smoothing of the spectral estimates because the large time lags involved when considering mantle structure appear as a high frequency modulation on the spectra.

1.3 Observed Spectral Ratios

The inversion of P-wave spectral data involves the calculation of the ratio of the vertical and horizontal components of ground motion in the frequency domain. This ratio involves both phase and amplitude information and is, therefore, a complex quantity; so for comparison purposes, the modulus or absolute value of the ratio is generally considered alone.

A simple Fourier transform of the seismogram would yield its complex spectrum, however, for reasons considered below, it is more convenient to consider the power spectrum of the seismic data. As noted above, the mantle of the earth is possibly a cause of multiple reflections and conversions of teleseismic wave prior to their arrival at the base of the crust. Such a mantle structure has large time lags associated with it, and close spectral peaks, while the effect of crustal layers on the spectrum should be small time lags and widely spaced spectral peaks. Figure A-1 shows theoretical spectral ratios for simple 2-layer models of various thicknesses, but with identical layer velocities. The thicker the model, the closer the spectral peaks approach each other. The use of the power spectrum in the analysis rather than

the simple Fourier transform allows one to smooth the resulting spectrum and thus eliminate any mantle structure from the problem. Ellis and Basham (1968) carried this smoothing procedure even farther and proceeded to remove not only the effect of mantle structure from the spectrum but also the effect of the whole lower crust.

In practice, the maximum time lag which can be considered in the power spectrum is equal to the length of the P-coda under consideration because the power spectrum is a Fourier cosine transform of the autocorrelation function of the data. Only lags from zero to some finite value are available so the autocorrelation is only an estimate. One must, therefore, effectively multiply the true autocorrelation with infinite lag by a time window of the same length as the available data.

1.4 Theoretical Spectral Ratios

Since a time window must be applied to the observed data, a similar window should be applied to the theoretically determined spectral ratios. LeBlanc (1966), the first to study this problem in detail, showed that comparing the theoretical truncated spectral ratio to the observed truncated spectral ratio was a valid process provided the source was short compared to the record length. Alpaslan (1968) gave a straight forward means of generating truncated theoretical spectral ratios. He convolved an assumed source with the theoretical transfer functions to yield vertical and horizontal component synthetic seismograms. These synthetics were then treated precisely in the same manner as the observed seismograms, that is, the same time window was chosen, and the power spectral ratios calculated in the same way. This process results in the comparison of theoretical and experimental results both

of which have undergone exactly the same type of processing. This method was used in this study although, for the length of window used (forty seconds) and in the frequency range of 0.5 to 4.0 Hz, the difference between the truncated and non-truncated theoretical spectral ratio was found to be actually insignificant.

CHAPTER II

EXPERIMENTAL DATA

2.1 Introduction

In the fall of 1969 an array of three seismograph stations was operated by The University of Alberta in the area immediately south-east of the town of Leduc, Alberta. Each station consisted of a three component broad band seismic system recording directly on seven track digital tape. The system is described in detail in Burke, Kanasewich, Malinsky, and Montalbetti (1970). Basically it is composed of Willmore MK II seismometers with natural periods of 1.5 seconds and an electronic amplifier which extend the usable velocity sensitivity out to the 40 second period range under normal conditions. This system response is obtained by the use of second order active RC network filters and low noise amplifiers which separate long and short period data, amplify the long period data to compensate for the drop in sensitivity due to the seismometer, and, then, recombine the two signals in such a way as either to enhance or attenuate microseismic noise. An analog to digital converter was used to record the data on a seven track digital field tape.

The amplifiers were calibrated and matched in the laboratory but no calibration was undertaken of the whole system including the seismometers. Hence there is some uncertainty as to the relative amplitudes of the components of the various events at the three field stations. Careful calibration must certainly be done in the future for spectral ratio work which involves amplitude ratios of different systems at different frequencies.

The microseismic attenuation feature of the system proved to be unfortunate from the point of view of studying spectral ratios and no useful long period spectral ratio data greater than two second period was obtained in the fall of 1969. The higher frequency range (0.5 to 3.0 Hz) produced good data, however, particularly for studies of the upper crust.

Four events, all from the Aleutian Islands, were chosen for spectral ratio studies. Pertinent information about these events is shown in Table 2-1. Inspection of the seismograms show them all to have a high signal to noise ratio. Since all the events come from the same area, no discrepancies from either difference in angles of incidence or azimuthal inhomogeneities around the station are expected. Inspection of travel time charts shows that for the epicentral distance of about forty degrees, no S-waves generated at the source can be expected for almost six minutes after the onset of the P-waves; the PP-wave is delayed about one hundred seconds; and the PcP over two minutes. Hence these phases are not expected to interfere with the initial P-coda.

TABLE 2-1

EVENT	DATE	MAGNITUDE	EPICENTRAL DISTANCE	DEPTH	AZIMUTH AT OBS	STATIONS RECORDING
Amchitka Nuclear Test No. 1	2 Oct. 1969	6.5	39.0°	---	294°	OBS, VNG
Aleutians No. 2	18 Oct. 1969	5.6	42.3°	24 KM	295°	OBS, OSC, VNG
Andreanoff No. 3	21 Oct. 1969	5.9	39.1°	48 KM	299°	OBS, OSC, VNG
Aleutians No. 4	31 Oct. 1969	6.0	39.0°	49 KM	294°	OSC, VNG

2.2 The Effect of the Phase pP

The earthquakes chosen occur at depth, and pP phases are expected only seconds after the P impulses. Phinney (1964) has studied the effect of pP phases on the spectral ratios and concluded that, provided the amplitude of these phases are small in comparison with the initial pulse, they will not affect the validity of the analysis since the signal will retain its random nature. If the pP phase is significantly large, however, a perturbation ripple with a frequency spacing of one over the pP-P time lag will show up on the spectrum. To test for the existance of this perturbation on the spectral ratios, an experiment was performed on data obtained at the OSC station. A cepstrum analysis of the observed spectral ratio, as used by Bakun (1971), was performed to separate those recurring features having a close frequency spacing from those having a longer frequency spacing. It is interesting to note that such an analysis has units of cycles per hertz or, simply, seconds. Hence, one can obtain from the cepstrum a graph of the amplitude of the spectral ratio versus the time lags which have presumably produced the characteristics of the transfer function. Short time lags would, for instance, arise from the sedimentary layers of the crust, longer time lags from the structure of the deep crust, and the longest time lags from the mantle structure. If the pP phase significantly perturbs the spectral ratio, then, much information from the lower part of the crust might be lost due to interference from the pP effect. Figure A-2 shows the cepstrum curve for the OSC events. Two of the events, OSC 3 and OSC 4 occurred at depths of 48 KM, thus, giving rise to a pP phase arrival at about twelve seconds after the initial P. This phase can be identified on the records quite well. The curve does

show peaks for the OSC 3 and OSC 4 events at the predicted time lag of about twelve seconds. The OSC 2 event, however, which occurred at a depth of only 24 KM with a pP-P lag of six seconds has a quite different curve for time lags greater than five seconds which suggests that the similarity between the curves of OSC 3 and OSC 4 is not due to the similar lower crust beneath them since the crustal effect would have influenced OSC 2 as well. The pP-P effect on the spectral ratios is, thus, seen to be significant, and may, indeed, be a more important source of the close-spaced ripples on the ratios than the lower crustal structure. It would be possible to avoid this effect by choosing for spectral ratio studies only those events which are very shallow such as nuclear tests or those events which are very deep such that the pP-P time lag would be so large as to not affect the P-coda window at all. In this study, concerned mostly with only the effect of the sediments on the spectral ratio, the perturbation ripples due to the pP-P lag are no larger than 0.2 Hz which would not affect the general characteristics of the spectral ratios. In fact, Figure A-2 shows considerable similarity between all three events for time lags less than five seconds which would be sufficient for any effects of the upper crustal layers.

2.3 Rotation of the Observed Data

Since the data was recorded using a tri-partite system aligned in the vertical, east-west, and north-south directions, the horizontal components of ground motion were first rotated to obtain a radial and transverse record. To accomplish this, the expected great circle azimuth from source to receiver was computed and a transformation was applied to the data as follows:

$$R = E \sin \phi + N \cos \phi$$

$$T = -E \cos \phi + N \sin \phi \qquad 2.1$$

where ϕ is the great circle azimuth measured clockwise from the north. R, T, E, and N are the radial, transverse, east-west, and north-south components of ground motion respectively.

Ideally, the P-coda should produce ground motion in the vertical and radial directions only for a crust consisting of horizontal layers. A certain degree of scattering in the crust, however, must be expected and, hence, there is motion in the transverse plane on the observed records. The transverse motion is generally small compared to the vertical and radial motion, however, and hopefully, the scattering does not affect the spectral ratios drastically.

Ellis and Basham (1968), by means of particle motion studies, have suggested that seismic waves arriving at Leduc are coming in at an azimuth averaging 18 degrees further north than predicted from the great circle path. An experiment was performed to test this assertion by an independent method and also to obtain more information about the transverse motion on the records. The north and south components were rotated in one degree increments and the maximum value of the autocorrelation function of the transverse trace was calculated for each azimuth angle. Since the autocorrelation function gives an estimate of the amount of energy in a trace, that azimuth angle for which the autocorrelation is minimum yields an apparent azimuth angle for each event. Table 2-2 shows those azimuth angles for which the maximum value of the autocorrelation function was a minimum for the various events at the three field stations.

TABLE 2--2

EVENT	STATION	ANGLE OF MINIMUM TRANSVERSE ENERGY
Amchitka	VNG	318°
Aleutians 18 Oct.	VNG	337°
	OBS	255°
	OSC	295°
Andreanoff	VNG	268°
	OBS	264°
	OSC	306°
Aleutians 31 Oct.	VNG	293°
	OSC	293°

The expected great circle azimuths for these events are in the 295° to 300° range. It is likely that since only a hand compass was used to orient the stations at OSC and VNG, there might be several degrees error inherent in these results, but the amount of scatter indicates that this method is probably not a very reliable means of obtaining the actual azimuth angle. However, it is interesting to note the very low azimuth angles at OBS. This phenomenon is perhaps indicative of a large amount of transverse energy being generated in the immediate locality of this station.

2.4 Spectral Analysis of the Field Data

Analysis of the rotated records indicated that useful P-coda information was arriving at least forty seconds after the first P pulse. At times later than forty seconds, the transverse trace appeared to have as much energy as the vertical and radial components and it was not felt that this later information would be very useful. Hence, the

first forty seconds of each event were used to obtain spectral ratios. To avoid a sharp edge on the end of the data, a cosine taper was used on the last four seconds of the forty second window. Actually, experiments showed that for a window this long the taper had very little effect on the final spectral ratios. Since a forty second P-coda necessarily includes the pP phase for medium depth Aleutian events, the spectral ratios were also calculated for a ten second P-coda. The ten second window, however, provided poor resolution of the spectral ratio. Figure A-3 shows the comparison for the October 31 event of spectral ratios with a ten second window and a forty second window. Since some of the larger peaks seen with the forty second window are quite narrow, it is reasonable to expect they might be diminished in the low resolution involved when one considers only ten seconds of data digitized at 0.08 second intervals.

The forty second P-coda contained 501 points to which an additional 523 zeros were added to bring the total number of points in the time sequence to 1024 for each trace. The autocorrelation of the vertical and horizontal components were computed. A Parzen window was applied to the autocorrelations for truncation purposes and, finally, the inverse Fourier transform of these modified autocovariances was performed to yield vertical and horizontal power spectrums for 512 points ranging from .01 Hz to 6.25 Hz. Fourier transforms and their inverses were computed using a high-speed algorithm developed by Gentleman and Sande (1966). The square root of the ratio of the vertical to horizontal spectrums at each frequency increment was then computed to yield the observed spectral ratios. Since it is possible that a particular event may have no energy at certain frequencies, a

rejection criteria should be used to avoid these frequencies. For the few events used in this study, both the vertical and horizontal spectrums were studied before the ratios were computed and no frequency voids were apparent.

2.5 The Reliability of the Observed Data

An interesting fact about spectral ratio studies is that at a particular station, totally different events at approximately equal epicentral distances should produce exactly the same P-coda spectral ratios regardless of the nature of the individual earthquakes. The actual observed spectral ratios for the aforementioned events at the three different stations are shown in Figures A-4, A-5, and A-6. The extent to which the spectral ratios are alike at each station is a measure of the reliability of the spectral ratio method. For the fall 1969 data, it is clear that at least the general character of the spectral ratios are significant at each of the three stations. The smaller "second order" peaks and troughs are less useful in that they change for the different events.

The reliability of the Leduc Observatory (OBS) data can be checked with data from other sources. Ellis and Basham (1968) and Jensen (1970) have previously recorded events at the Leduc Observatory in the forty degree epicentral range and have calculated the spectral ratios. Figure A-7 shows their spectral ratios compared with the Leduc ratios from this study. The agreement is quite good considering the large amount of smoothing used by the above researchers in their analyses.

Since it is desirable to have a single observed spectral ratio for each station for interpretational purposes, a non-linear filter was designed to combine the spectral ratios from the different events according to the following formulae:

C_j = value of the combined ratio

V_{ij} = value of the ratio of event i at frequency index j

$T_{ij} = V_{ij} - 1$ if V_{ij} is greater than 1

$$T_{ij} = \frac{-1}{V_{ij}} + 1 \text{ if } V_{ij} \text{ is less than 1}$$

N = strength of the combination

NE = number of events combined

$$S_j = \frac{1}{NE} \sum_{i=1}^{NE} \left[\left(\frac{T_{ij}}{|T_{ij}|} \right) \cdot |T_{ij}|^{1/N} \right]$$

$$R_j = \frac{|S_j|}{S_j} \cdot |S_j|^{N}$$

$C_j = R_j + 1$ if R_j is greater than 0

$$C_j = \frac{-1}{R_j - 1} \text{ if } R_j \text{ is less than 0} \qquad 2.2$$

The effect of this method of combining the data from the various events is to remove from the combined data those peaks and troughs which are not common to all the stations. The stronger the combination, the more

drastic is the removal of dissimilar character. For a filter strength of one, the combination reduces to simply an average of the events combined.

CHAPTER III

THE CRUSTAL MODEL FOR CENTRAL ALBERTA

3.1 Introduction

In order to generate a theoretical spectral ratio for any given crustal model, it is necessary to know the thickness, P and S velocities, and density in each assumed layer as well as the angle of incidence of the source wave at the base of the bottom layer. The complexity of the crust in central Alberta makes the determination of many of these parameters difficult. Even the basic number of layers required to properly represent the crust is not really known. This chapter is an attempt to resolve some of these difficulties and arrive at a suitable crustal model for central Alberta.

This region is geologically characterized by a thick flatly bedded sedimentary section dipping generally less than one hundred feet per mile to the southwest. In the area of The University of Alberta's Leduc Observatory, (Figure A-8), the lithology of the upper 2 KM of the sediments is well known due to extensive exploratory drilling into the Devonian reef zones. The Paleozoic section beneath the reef zone is much less known since few wells are drilled into these non-oil bearing depths. Three wells in the Edmonton area have penetrated the Precambrian basement. Interpolation between these wells gives the total thickness of the sediments at the Leduc Observatory to be about 2.7 KM, as shown by the basement structure contours in Figure A-8. Only two wells in the immediate vicinity of the observatory have had sonic logs run in them. One of these wells is fortuitously located almost on the line between the Leduc Observatory (OBS) and the two

temporary auxiliary stations OSC and VNG, hence, good control on P-wave velocity is expected. Unfortunately the sonic logs do not cover the upper 200 meters of the section nor any beds below the reef zone, so additional velocity information was obtained from reflection seismograms in the area. No published information is available for S-wave velocities, depth of weathering or layer densities.

Interpolation of the well data in the area yields the structure through the three stations as tabulated in Table 3-1. The P-wave velocities down to the Cooking Lake formation are an average of the two available sonic logs with more weight being given to the log nearest the stations. The P velocities in the lower sediments are from a seismic reflection survey shot in the area. The basement velocity is a value obtained from a regional refraction survey in southern Alberta (Kanasewich and Cumming, 1966).

Formation density information is not readily available. The effect of density on the spectral ratios is strictly one of amplitude, since the density affects the reflection coefficients of the various boundaries but not the speed nor direction with which the waves travel through the layers. Figure A-9 shows two theoretical ratios for typical nine layer Alberta sedimentary crustal models, the only difference between the models being the density distribution. The different density models produce identical ratios except for amplitude variations. Because density does not alter the character of the theoretical ratios, the P-wave velocity-density curve of Nafe and Drake was used to assign density values to the crustal layers.

The S-wave velocities in the sediments of central Alberta are not known. The usual assumption of rocks behaving as ideal Poisson

TABLE 3-1

THICKNESS (KM)			P-WAVE VELOCITY (KM/SEC)	DENSITY (GM/CC)
OBS	OSC	VNG		
.01	.01	.01	2.1	2.1
.60	.62	.64	2.3	2.1
.19	.21	.21	2.9	2.2
.10	.11	.11	3.15	2.2
.04	.04	.04	2.85	2.2
.04	.04	.04	3.30	2.3
.08	.08	.08	2.85	2.2
.04	.04	.04	3.70	2.3
.02	.02	.02	2.80	2.2
.13	.14	.16	3.40	2.3
.07	.08	.08	3.85	2.3
.15	.15	.19	5.80	2.6
.24	.18	.24	4.00	2.4
.21	.21	.21	5.20	2.6
.21	.21	.21	5.00	2.6
.52	.56	.58	4.30	2.5
---	---	---	6.10	2.7

TABLE 3-2

NAME	THICKNESS (KM)	P-WAVE VELOCITY (KM/SEC)	DENSITY (GR/CC)
POST ALBERTA	.61	2.30	2.1
ALBERTA	.51	3.00	2.2
BLAIRMORE	.20	3.54	2.3
WABAMUN	.15	5.80	2.6
IRETON	.24	4.00	2.4
CK LK	.21	5.20	2.6
ELK PT	.19	5.00	2.6
CAMBRIAN	.52	4.30	2.5
BASEMENT	---	6.10	2.7

solids with the P-wave velocity equal to 1.73 of the S-wave velocity was not necessarily considered reliable. The problem of assigning S-wave velocities will be considered in detail later. As a first approximation, the S-waves are given a velocity equal to one half of that of the P-waves. This ratio corresponds to a solid having a Poisson's ratio of one-third.

The initial sedimentary model involving seventeen layers is based on the analysis of the sonic logs. Because of the thinness of some of these layers, it was felt they would have little effect on the spectral ratios in the frequency range in question (0.2 - 4.0 Hz), so the seventeen layer crust was reduced to a nine layer crust as shown in Table 3-2. A nine layer crust is consistent with the crust assumed by Ellis and Basham (1968) and Jensen (1970) for central Alberta spectral ratios.

Figure A-10a shows the comparison between the theoretical spectral ratios for the seventeen layer crust at Leduc and the nine layer crust. They are almost exactly identical. The success of this experiment suggests an even further reduction of effective sedimentary layers to three as used by Alpaslan (1968). Figure A-10b shows the comparison between the seventeen layer model and the three layer model at Leduc. While there is remarkable similarity of the theoretical ratios at the lower frequencies, there are significant changes in the amplitude of the peaks and at the high frequencies the character of the ratio is quite different. This analysis resulted in the use of the nine layer model for most efficient and reliable studies of the effect of sediments on the theoretical ratios.

Figure A-11 shows the comparison between observed and theo-

retical spectral ratios based only on the sedimentary crust at Leduc as modelled above. There is little similarity between the curves. This result agrees with the findings of Ellis and Basham (1968) who explained this lack of agreement as probably due to scattering at the base of the crust. Another possible explanation, however, is a fundamental error in the crustal model.

Analysis of the structure beneath the three stations shows thickening of the sediments to the southwest. Fernandez (1966) has shown that all other parameters being the same, a thickening of the model should cause the peaks of the spectral ratios to migrate toward smaller frequencies since those waves which are able to constructively and destructively interfere in the thicker crust must have a longer wavelength. This effect is demonstrated in Figure A-1 for a very simple two layer crustal model. As the thickness of this crust is increased the peaks migrate to lower and lower frequencies. As predicted from the thicknesses of the sediments, VNG located on the thickest sediments of the three stations should have peaks offset toward the lower frequencies, OBS on the thinnest sediments should have peaks toward the higher frequencies, and OSC station should be in between. Figure A-12 shows the actual results at the three field stations. The various peaks do not migrate as predicted, hence other factors than simple thickening must be affecting the spectral ratios differently at the three stations.

3.2 Weathering Layer Effects on the Spectral Ratio

A possible explanation for the difference in the observed spectral ratios at the three stations and for lack of agreement between

experimental and theoretical results was thought to be changes in the low velocity weathering layer. Bayrock and Hughes (1962) have studied the surficial geology of the Edmonton area. The bedrock in the Leduc area is composed of upper Cretaceous shales, shaly sandstones, and sandstones which dip twenty feet per mile to the southwest. This bedrock is overlain by eight to ten feet or more of glacial drift. The three stations are located in an area called the Gwynne Outlet produced by the erosive action of escaping waters from Pleistocene Lake Edmonton. A shaly sand deposited in the Gwynne Outlet varies from one to five feet in thickness and is now on the surface at the stations. The exact depth of the till at the stations was not known, and a hammer seismograph survey was performed to determine the depths and velocities of the surficial material at the OBS station. The upper ten feet was found to be very low velocity material, 1250 feet per second, perhaps the shaly sandy soil mentioned above. The interval from ten to thirty feet in depth has an average velocity of 4300 feet per second and is probably glacial till. 6700 feet per second material was found at a thirty foot depth and is possibly bedrock. The horizontal extent of this refraction survey was only about four-hundred feet, hence, it is possible that more surficial layers than are indicated above are present. Furthermore, any surficial layer of velocity lower than the layer above it could not have been detected by the refraction method used in the survey.

Spectral ratios were theoretically computed for models including surficial layering and were compared with the same models without the weathering layer. Using the hammer seismograph results and a usual Poisson's ratio, almost no weathering layer effect was noted on the spectral ratios. However, following Erickson et al (1968), a ratio

of S to P velocities of 1/6 was used as an extreme case for the unconsolidated surface layers to a depth of .02 kilometers resulting in the spectral ratios shown in Figure A-13. Two observations can be made:

1) The character of the ratio at higher frequencies is more affected by surficial layering than at lower frequencies. This effect was expected considering the very short time lags involved in multiple reflections within the weathering layer.

2) The effect of the weathering layer is to lower the amplitude of the spectral ratio over most of the frequency range. This phenomenon is mildly surprising since one would expect a low velocity surface layer to refract the incoming P-coda into a more vertical direction, hence, resulting in a higher vertical to horizontal surface motion ratio. However, because of the high Poisson's ratio possible in unconsolidated surficial material, it is the converted S-waves which become more important. When an S-wave is refracted toward the vertical, its transverse particle motion will result in a decrease of the ratio of vertical to horizontal surface motion.

The weathering layer is, therefore, seen as a possible important factor in spectral ratio studies in regard to the amplitude of the peaks, but not very significant as to the relative position of the peaks. Ellis and Basham (1968) experienced some difficulty in obtaining matches between theoretical and experimental ratios at several stations because of the high amplitude of their theoretical ratios. It is conceivable that the surficial layers at these stations might have had a considerable effect on the observed data and might have altered spectral ratio amplitudes considerably.

3.3 Poisson's Ratio in Sedimentary Rocks

In previous work on modeling the sedimentary crustal section (Ellis and Basham, 1968), the rocks have been assumed to be ideal Poisson's solids with a Poisson's ratio of 1/4. There have been few actual field measurements to verify this assumption, however. If Poisson's ratio is not held at 1/4, a considerable change in the theoretical spectral ratios can be expected. Koefford (1955) studied the effect of Poisson's ratio on the reflection coefficients of plane waves. His calculations for angles of incidence in the range 0° to 30° showed significant effects on the reflection coefficients which increased with the larger angles of incidence and decreased with smaller compressional velocities. From elasticity theory, it is well known that the ratio of compressional to shear wave velocity in a rock depends only on Poisson's ratio. The S-wave velocity is seen to contribute significantly to the spectral ratio. Calculations indicate that peaks in the horizontal transfer function and, therefore, troughs in the theoretical spectral ratios occur exactly at those frequencies for which the S-wave is able to reinforce itself after one or more reflections off the free surface (Fernandez, 1966). Hence Poisson's ratio for its effect both on reflection coefficients and on S-wave velocity is an important factor to be considered carefully when constructing crustal models for the sedimentary layers.

Koefford, Oosterveld, and Galons, (1963), made laboratory measurements of the P and S velocities of twenty-nine limestones of varying porosity. They found that Poisson's ratio decreased with increasing velocity and increased with water saturation. For water

saturated rocks of porosity less than 10%, not an untypical case for central Alberta sediments, the average value of Poisson's ratio was .311. Zisman (1933) made laboratory measurements on Poisson's ratio and concluded that "Poisson's Ratio increases greatly with mean stress applied", an observation that could have considerable bearing on assigning Poisson's ratios to deeply buried sedimentary rocks.

The difficulty in measuring Poisson's ratio in situ is mostly in efficiently generating S-waves at the source. Oliphant (1950) attempted to identify transverse body waves by shooting vertical profiles with a three component seismometer on the surface near a borehole and with shots at various depths in the borehole, thus, any transverse motion on the surface would have been due to shear effects. The experiment was not a success: "Evidently the fraction of detonation delivered to shear waves was exceedingly small in comparison with that delivered by other extraneous motions."

Richards (1933) gives P and S velocities from near surface measurements in Southwest Persia for overburdens consisting of sandstone, marls, anhydrite, salt, and limestone. The ratio of P to S velocity ranged from 1.8 to 2.3 with an average of 2.0, which corresponds to a Poisson's ratio of 1/3. Richards (1961) then proceeded to use a Poisson's ratio of one-third in analysing wide angle reflection data in the Alberta foothills.

Meizner (1965), Molotova (1963), and Okado (1964) have also made near surface in situ measurements of Poisson's ratio. They reported shear to compressional wave velocity ratios as low as 1/7 for low velocity weathering layers.

With the advent of mechanical vibrators, significant progress

has been made in recent years in determining S-wave velocities at depth. Cherry and Waters (1968) describe one such experiment, "In the field, the vibrator generates horizontal motion in the ground while suitable geophones are arranged to pick up this motion. SH waves are received if the source motion and geophones axes are at right angles to the spread direction. In a simple parallel layered system, SH is reflected and refracted as SH only and gives rise to a simple reflection record." In Medford, Oklahoma such shallow reflections indicated a Poisson's ratio of .394. They found that for most of the reflection examples, the average ratio of shear velocity to compressional velocity in the first few thousand feet was near .5, that is, Poisson's ratio was equal to 1/3.

The continuous signal method utilizing a mechanical vibrator was applied to borehole measurements by Erickson, Miller, and Waters (1968). They set up the vibrator to generate S-waves downward from the surface and lowered a geophone to various depths down to ten-thousand feet to record the signal. Interval (shear to compressional velocity) ratios were calculated from the combination of downhole S-wave data and continuous velocity log data. The values ranged from .45 to .70 with an average overall of .52, an average Poisson's ratio slightly greater than 1/3.

Figure A-14 shows the theoretical spectral ratios for the nine layer Leduc model for values of Poisson's ratio varying from .25 to .38. Superimposed on each of these is the OBS field data. While none of the models produce a satisfactory fit, the models with Poisson's ratio about .33 seem to be best.

Using Keofford's et al (1963) assertion that Poisson's ratio

decreases with increasing velocities as a basis, a nine layer crustal model was computed using a Poisson's ratio of .25 in hard layers (P-wave velocities greater than 4.0 KM/sec.) and .33 in soft layers (P-wave velocity less than 4.0 KM/sec.). This model is shown in Figure A-15a along with a model all layers of which have a Poisson's ratio equal to one-third. The difference between these two models is small indicating that it is the lower velocity layers in the sediments which are most strongly influencing the spectral ratios, at least, in so far as S-wave velocity is concerned.

Hence, it has been shown that Poisson's ratio can have a pronounced effect on the spectral ratios and S-wave velocities must be chosen carefully when modelling the sedimentary crust. However, it must be noted that no value of Poisson's ratio produces a match between observed and theoretical ratios for models based on only the sedimentary crustal layers at Leduc.

3.4 Effect of Anisotropy on the Spectral Ratio

Another possible cause for the lack of agreement between theoretical and observed spectral ratios might be anisotropy in the crustal layers. In general, the array of moduli of elasticity relating stress to strain in an elastic body is given by a symmetrical six by six matrix containing twenty-one independent terms. The strain energy function for such a body is a homogeneous quadratic function of six variables. These parameters may be simplified for homogeneous substances which have some degree of symmetry. If the body possesses symmetry in all directions so that the strain energy function is invarient to all transformations of axes, the body is said to be isotropic. Otherwise

it is anisotropic or aleotropic. A transversely isotropic media possesses an axis of symmetry in the sense that all rays at right angles to this axis are equivalent. Such symmetry is possessed geometrically by certain crystals of the rhombohedral and hexagonal systems. From the large scale seismic point of view, this is the symmetry found in flat sedimentary layers and planar igneous bodies. White (1955) and Postma (1955) have shown further that a stratified section composed of alternating layers of different elastic materials may be considered as a single homogeneous transversely isotropic layer for wavelengths large compared to individual layer thicknesses. Hence, transverse isotropy can be expected to arise in crustal layers from two sources, either the nature of the rock material itself or the manner in which thin isotropic rock layers are stratified.

Stonely (1949) was one of the first to study plane waves in a transversely isotropic media. Musgrave (1954), Postma (1955), and Jolly (1956) added the theory of anisotropic waves emanating from a point source. These authors indicated that the major differences between wave propagation in transversely isotropic media and in purely isotropic media are that, in the anisotropic body, there exists dependence of wave velocity on direction of travel and the waves do not separate into perfect P and S types, that is, waves for which the divergence or curl of the displacement vanish respectably. A derivation of velocities in a transversely isotropic medium is given in the appendix.

The fact that rocks are not isotropic has been observed for many years. Koefford et al (1963) determined longitudinal and transverse velocities of twenty-nine limestones of varying porosity and the elastic anisotropy factor, that is, the ratio of transverse velocity to longi-

tudinal velocity, was found to vary over a wide range from 0.8 to 1.6, a third of which were over 1.05. Layat et al (1961) noted that in order to satisfactorily identify refractions from marker beds in the Sahara, it was necessary to take anisotropy into account, for without anisotropy, depth calculations put marker beds in the middle of known homogeneous beds without velocity differentiations. Cherry et al (1968) from studies of shear wave propagations, determined an anisotropic factor of 1.08 for the upper sedimentary section in Medford, Oklahoma. Dunoyer de Segonzac and Leherrere (1959) determined anisotropic factors in the northern Sahara ranging from 1.00 in sandstones to 1.20 in andhydrite by a method utilizing a velocity log together with the first arrival times recorded at several geophone levels from shotpoints at various distances from the well. Vanderstoep (1966) utilized a similar method in New Mexico and Texas. The red beds in a 2400 foot well in Lea County, New Mexico showed anisotropic factor of 1.07, the salt beds 1.00. On the Texas Gulf coast, a 12,000 foot well yields anisotropic factors of 1.03 or less. McCollum (1932), Weatherby (1934), Ricker (1953), and White and Sengbush (1953) working in Canada, Oklahoma, Colorado, and Texas respectively, observed near surface anisotropy in shales and limestones ranging from 1.1 to 1.4. J. Cholet and H. Richard (1954) determined an anisotropic factor of 1.09 in the northern Sahara down to 1250 meters. A.H. Kleyn (1956) employed the results from a refraction profile, a well velocity survey, and a radial well survey in Betun, South Sumatra. He concluded that the anisotropic factor was 1.00 at the surface, 1.15 at 1500 meters, and 1.04 deeper. He further noted that, at great depths, the horizontal velocity may locally decrease or remain constant even though the vertical velocity increases

with depth. Anderson (1961) noted that anisotropy may be responsible for certain discrepancies in surface wave data including disagreements between Love wave and Rayleigh wave studies of both velocity and particle motion.

In order to calculate the theoretical spectral ratio for body waves in a system of transversely isotropic layers, the matrix method of Haskell (1953) can be used provided the terms involving elastic constants are properly modified beforehand. Anderson (1961) and Anderson and Harkrider (1962) were the first to apply the Haskell method to transversely isotropic media for the purpose of doing surface wave dispersion studies. A brief outline of the application of the Haskell matrices to body waves in a transversely isotropic layered system as conceived by E.R. Kanasewich of The University of Alberta is given in the appendix. This derivation leads to a matrix formula for calculating the theoretical ratio for P-waves which is particularly suitable for the digital computer.

Due to the low angles of incidence which P-waves from teleseismic events impinge on the crust, it is reasonable to expect that the effect of anisotropy on the spectral ratios will be small for such events since the direction of wave propagation is essentially vertical in these cases, and the horizontal velocities are only slightly brought into play. Figure A-16a shows the comparison of the theoretical spectral ratios for an isotropic model and an anisotropic model for the sedimentary layers at Leduc for an anisotropic factor of 1.2 and an angle of incidence of 20°. While a fair amount of change in amplitude of the peaks is noted, there is almost no frequency shifting of the peaks. Figure A-16b shows the same models at an angle of incidence of 40°.

Once again a significant change in the amplitude of the peaks is evident, but not so much as to change the overall character of the ratio. However, at an angle of incidence of 60° as shown in Figure A-16c, both the amplitude and position of the peaks are severely affected by anisotropy.

At larger angles of incidence, however, anisotropy is important and must be taken into consideration. Several researchers (Alpaslin, Ellis and Basham) have noted difficulties in obtaining reasonable matches between theoretical and experimental ratios for near events. Formerly this has been explained by anomalous SV conversions and simultaneous arrivals of energy from different ray paths. To these theories must be added the strong effect of anisotropy on waves arriving at such large angles of incidence.

Figure A-15b shows the comparison of the isotropic and anisotropic models at Leduc for an angle of incidence of 26° which is thought to be the actual case for earthquake epicenters in the Aleutians. The difference is, as expected, mostly only a matter of amplitude although at a frequency of just under 2.0 Hz a small peak does appear on the anisotropic ratio which was not present on the isotropic ratio. It is evident that at this angle of incidence it is not likely that anisotropy could be the cause of any large discrepancies in character between theoretical and observed spectral ratios.

3.5 Effect of Deep Crustal Layering

It is probable that the sedimentary structure alone can account for neither the general character of the observed spectral ratios nor

the change in the character of the ratios from station to station. Before disregarding the spectral ratio method, however, one should consider the possibility of deeper layers in the crust affecting the spectral ratios. Ellis and Basham (1968) have shown that the addition of the "gross" crustal layers, that is, those layers between the sediments and the Mohorovicic discontinuity, does not have a significant effect on the general characteristics of the spectral ratios. The deep crustal layers added were a generalization of those given by Kanasewich and Cumming (1966) as the results of regional refraction studies in southern Alberta. Figure A-17a shows the theoretical spectral ratios for a model consisting only of the sediments at Leduc and for a model of the sediments plus the deeper crustal layers used by Ellis and Basham. The two ratios are quite similar in general characteristics. The effect of the deep layers is the addition of small oscillations on the general curve shape. These small oscillations are not apparent on a similar comparison given by Ellis and Basham (1968) probably because of the large amount of smoothing performed in their analysis. The presence of the small oscillations is in agreement with the work of Phinney (1964) who predicted that any layer would produce oscillations on the spectral ratios with frequency spacing equal to one over the associated time lag.

Hence the deeper crustal layers because of their long time lags (the two way time to the Mohorovicic discontinuity, for example, is about twelve seconds) should produce oscillations with very short frequency spacings. This apparent failure of the deeper crustal layers to affect the spectral ratio coupled with the lack of correlation success with spectral ratios based on only the sediments, leaves

only one possibility for successful application of the method, that is, intermediate crustal layers in the upper few kilometers of the pre-Cambrian rocks.

3.6 Models Involving a Shallow Thin Soft Layer in the Pre-Cambrian

The pre-Cambrian in Alberta has been studied by Burwash (1957), Garland and Burwash (1959), and Kanasewich and Clowes (1969). Burwash (1957) presented data from petrological studies of pre-Cambrian core samples showing that the rock types in the basement vary considerably in different localities. A well in the Leduc area actually contained two different rock types in the upper few feet of the basement complex. Garland and Burwash (1959) combined petrological and geophysical data to produce a rough lithological map of the basement in central Alberta. Kanasewich and Clowes (1969), utilizing deep seismic sounding and gravity data in southern Alberta mapped a rift in the pre-Cambrian extending down to the Mohorovicic discontinuity. The pre-Cambrian in Alberta is, hence, seen to be a complex geological system rather than a homogeneous crystalline substance as often supposed. It is not unreasonable, therefore, to suggest the existance of layering in the uppermost basement rocks which could have a significant effect on the spectral ratios.

An initial attempt to arrive at a suitable theoretical spectral ratio to match the observed data at Leduc by means of an additional layer in the basement was based on three factors: 1) Visual inspection of the observed ratios indicated that a better match could be obtained if the theoretical peaks were shifted toward lower frequencies. Fernandez (1965) noted that it is possible to perform such a shift by

increasing the depth of the model. One method of increasing the depth is the addition of another layer on the bottom of the sediments. 2) The gravity map of central Alberta shows the Leduc area to be located in the center of a broad gravity low. A shallow "soft" layer in the basement could explain such a low. 3) Commercial seismic reflection operations in the Edmonton area often fail to produce any clear reflection from the basement surface. A possible explanation for this phenomenon could be a low reflection coefficient at the top of a "soft" basement layer.

Several hundred theoretical spectral ratios were generated using models with an additional layer on the bottom of the sediments, the best of which is shown in Figure A-17b along with the observed ratio at OSC station. The fit is apparently reasonable. The model involves a soft layer of about 2000 feet thickness beneath the sediments. Unfortunately, no suitable models were found to fit the data for the other stations as well, hence, the fit for the OSC data is probably nothing more than a good illustration of the ambiguity of the inversion process.

3.7 A Three Second Marker in the Pre-Cambrian

Evidence for a possible marker bed in the pre-Cambrian at a two-way time of 3.0 to 3.5 seconds comes from two independent sources. Referring back to Figure A-2, the cepstrum analysis of observed spectral ratios at OSC stations, one can note an interesting phenomenon. The graphs show the effect which difference in time lags have on the spectral ratios. The time lag which would probably have the most effect

on the observed ratio is the two-way reflection time for various markers in the layered system. The three graphs, each for a different event recorded at the same stations, show remarkable similarities for short time lags, that is, short two-way times undoubtably associated with sedimentary layers. It is very interesting that the similarity between the three events continues out to about 3.5 seconds, while the total two-way time in the sediments around Leduc is less than 1.6 seconds. One explanation for the significant time lag at 3.5 seconds could be multiples within the sediments, but a more interesting possibility is the existance of a true marker in the pre-Cambrian at a two-way time of around 3.5 seconds.

Recent deep seismic reflection records from the area several miles north of the Leduc Observatory obtained by G. Cumming of The University of Alberta have indeed shown a distinct reflection at a two-way time of 3.4 seconds.

The generation of theoretical spectral ratios for models with a marker in the 3.0 to 3.5 second range can lead to various possibilities for the thickness and P-velocity of the basement layer since it is only the ratio of the terms, the transit time, which is known. Hence, the spectral ratio method could be of considerable use in determining the actual thickness of the basement layer, if the various models do not prove to be completely non-unique.

At the Leduc Observatory, no satisfactory fit was obtained with any model involving a 3.4 second marker, however, a reasonable fit was obtained with a 3.1 second marker as shown in Figure A-18a. The essential feature of this model is the low P-wave velocity used in the basement layer (4.6 KM/sec.). This low velocity keeps the reflection

coefficient at the bottom of the sediments small. Figure A-19b shows the theoretical ratios for a two-way time of 3.1 seconds for models with higher P-velocities in the basement. The models become more and more like the theoretical ratio for a model based only on the sediments as the reflection coefficient at the basement surface is increased.

Further encouragement for the 3.0 second marker models comes from a reasonable fit for the VNG station as shown in Figure A-19a. While the fit is by no means excellent, it is by far the closest of any of the hundreds of models in this study attempted for the VNG station. This particular model is for a pre-Cambrian marker at 3.0 seconds or only 0.1 second different from the OBS station which is located some twelve miles away.

To see if the lower crustal layers might improve the fit for the 3.1 seconds model at OBS, the presumed Conrad and Mohorovicic discontinuities were added to the model, and the resultant spectral ratios are shown in Figures A-18b and A-18c. The closely spaced modulations due to these layers do not alter the theoretical spectral ratios to an important degree.

No fit was found for the OSC station, however, which is located between the other two stations, six miles distant from each. This lack of a match may indicate a great deal of complicated structure in the pre-Cambrian basement in the Leduc area, or it could also point out the inherent non-uniqueness and consequent lack of certainty in the matches at the OBS and VNG stations. A detailed gravity survey is currently being undertaken in hopes of gaining more information about the sub-basement structures, if any, in the Leduc area.

The models which most closely fit the OBS and VNG data produce

theoretical spectral ratios which are too high in amplitude. Ellis and Basham (1968) have encountered a similar problem, tentatively explaining the low observed ratios as due to scattering and anomalous P to S conversions near the base of the sediments. Another possible explanation might be as discussed in section 3.2, effects of non-consolidated near surface sediments with an extremely high Poisson's ratio. At any rate, the problem of the amplitude difference between observed and theoretical spectral ratios in the Leduc area remains unsolved at this time.

3.8 Future Spectral Ratio Studies

The spectral ratio method in the high frequency range has been found to be potentially very sensitive to two parts of the crust which are often overlooked in other types of seismic investigations, namely, weakly consolidated surficial layers and relatively shallow structures in the crystalline basement. The method could prove to be a very valuable mapping tool for these types of studies in the future.

For investigations of the lower crust, however, the high frequency spectral ratio inversion is unsuitable. Future spectral ratio studies of the deep crust should probably involve longer period data from only carefully selected events in order that the effects of shallow crustal layering and of pP type phases might be minimized.

One of the more interesting lessons to arise from these studies into the spectral ratio method was the surprising difficulty encountered in obtaining even a few plausible matches between theoretical and observed data considering the limited frequency range, the considerable

number of free parameters, and the inherent non-uniqueness of the problem. This observation indicates that the most efficient and instructive method of handling such inversions in the future might be based on a computerized curve matching technique since the apparent scarcity of good fits would make any good match, based on a model consistent with the known geology, worth further investigation.

BIBLIOGRAPHY

Alpaslan, T. 1968 Spectral Behavior of Short-Period Body Waves and the Synthesis of Crustal Structure in Western Canada. Thesis, The University of Alberta, Edmonton, Alta.

Anderson, D.L. 1961 Elastic wave propagation in layered anisotropic media. J. Geophys. Res., 66, pp. 2953-2963.

Bakun, W.H. 1971 Crustal model parameters from P-wave spectra. Bull. Seis. Soc. Amer., 61, pp. 913-936.

Bayrock, L.A. and Hughes, G.M. 1962 Surficial Geology of the Edmonton District, Alberta. Research Council of Alberta Preliminary Report 62-6.

Burke, M.D., Kanasewich, E.R., Malinsky, J.D., and Montalbetti, J.F. 1970 A wide-band digital seismograph system. Bull. Seis. Soc. Amer., 60, pp. 1417-1426.

Burwash, R.A. 1957 Reconnaissance of subsurface Precambrian of Alberta. Bull. Amer. Assoc. of Petr. Geol., 41, pp. 70-103.

Cherry, J.T. and Waters, K.H. 1968 Shear wave recording using continuous signal methods. Part 1: Early Development. Geophysics, 33, pp. 229-239.

Cholet, J. and Richard, H. 1954 A test on elastic anisotropy measurement at Berriane (North Sahara). Gph. Prospecting, 4, pp. 232-246.

Dunoyer de Segonzac, P. and Leherrere, J. 1959 Application of the continuous velocity log to anisotropy measurements in the northern Sahara; results and consequences. Gph. Prospecting, 20, pp. 780-806.

Ellis, R.M. and Basham, P.W. 1968 Crustal characteristics from short period P-waves. Bull. Seis. Soc. Amer., 58, pp. 1681-1700.

Erickson, E.L., Miller, D.E., and Waters, K.H. 1968 Shear wave recording using continuous signal methods. Part II: Later experimentation. Geophysics, 33, pp. 240-254.

Fernandez, L.M. 1965 The determination of crustal thickness from the spectrum of P-waves. Scientific Report No. 13, Contract AF 19 (604) 7399, Project 865201.

Fernandez, S.J., Rev. L.M. 1966 The Determination of Crustal Thickness from the Spectrum of P-Waves. Thesis, St. Louis University, St. Louis, Missouri, 192 pp.

Garland, G.D. and Burwash, R.A. 1959 Geophysical and petrological study of the Precambrian in Central Alberta. Bull. Amer. Assoc. of Petr. Geol., 43, pp. 790-806.

Gentleman, W.M. and Sande, G. 1966 Fast Fourier transforms - for fun and profit. Proc. of the Fall Joint Computer Conference, San Francisco, pp. 563-578.

Gutenberg, B. 1934 Periods of the ground in southern California earthquakes. Earthquake Investigations in California: 1934-1935, U.S. Coast and Geodetic Survey, Spec. Publ. 201, pp. 163-225.

Gutenberg, B. and Richter, C.F. 1936 Deep focus travel time curves. Material for the study of deep focus earthquakes. Bull. Seis. Soc. Amer., 26, pp. 341-390.

Harkrider, D.G. and Anderson, D.L. 1962 Computation of surface wave dispersion for multilayered anisotropic media. Bull. Seis. Soc. Amer., 54, pp. 377-393.

Hasegawa, H.S. 1971 Crustal transfer ratios of short and long-period body waves recorded at Yellowknife. Bull. Seis. Soc. Amer., 61, pp. 1303-1320.

Haskell, N.A. 1953 The dispersion of surface waves on multilayered media. Bull. Seis. Soc. Amer., 43, pp. 17-34.

Jensen, O.G. 1970 Linear Systems Theory Applied to a Horizontally Layered Crust. Thesis, University of British Columbia, Vancouver, B.C.

Jolly, R.N. 1956 Investigation of shear waves. Geophysics, 21, pp. 905-938.

Kanasewich, E.R. and Clowes, R.M. 1969 A buried Precambrian rift in western Canada. Tectonophysics, 8, pp. 513-527.

Kanasewich, E.R. and Cumming, G.L. 1966 Crustal Structure in Western Canada. Final Report, Contract No. AF 19 (628) 2835, Project No. 8652, Task No. 865202.

Kleyn, A.H. 1956 On seismic wave propagation in anisotropic media with applications in the Betun Area. Gph. Prospecting, 4, pp. 56-69.

Koefford, O. 1955 On the effect of Poisson's ratio of rock strata on the reflection coefficients of plane waves. Gph. Prospecting, 3, p. 381.

Koefford, O., Oosterveld, M., and Galons, I. 1963 A laboratory investigation into the elastic properties of limestone. Gph. Prospecting, 11, pp. 300-312.

Layat, C.A., Clement, A.C., Pommier, G., and Buffet, A. 1961 Some technical aspects of seismic refraction prospecting in the Sahara. Geophysics, 26, pp. 437-446.

Leblanc, G. 1966 Spectral Analysis of Short Period First Arrivals. Thesis, Pennsylvania State University, University Park, Pa.

Love, A.E.H. 1945 The Mathematical Theory of Elasticity. 4th ed., Cambridge U. Press.

McCollum, B. and Snell, F.A. 1932 Asymmetry of sound velocity in stratified formations. Reprinted in: Early Geophysical Papers, Society of Exploration Geophysicists, 1947, pp. 212-217.

Meizner, P. 1965 P and SV waves from uphole shooting. Abstracts of EAEG meeting, Gph. Prospecting, 13, p. 140.

Molotovna, L.V. 1963 Velocity ratios of longitudinal and transverse waves in terrigeneous rocks. Bull. (Izvestiya) Acad. Sci. USSR. Gph. Ser. No. 12, p. 1769.

Musgrave, M.J.P. 1954 On the propagation of elastic waves in aelotropic media. Proc. Roy. Soc., 226, pp. 339-366.

Neumann, F. 1954 Earthquake Intensity and Related Ground Motion. University of Washington Press, Seattle, 77 pp.

Okado, H. 1964 Analyses of seismic waves generated by small explosions. J. of Faculty of Science, Hokaido University, Japan, Series 7, 2, p. 197.

Oliphant, C.W. 1950 Seismic velocities in sedimentary rocks. Bull. G.S.A., 61, pp. 759-788.

Phinney, R.A. 1964 Structure of the earth's crust from spectral behavior of long-period body waves. J. Geophys. Res., 69, pp. 2997-3017.

Postma, G.W. 1955 Wave propagation in a stratified medium. Geophysics, 20, pp. 780-806.

Richards, T.C. 1933 On the elastic constants of rocks with a seismic application. Proc. of the Phys, Soc. (London), 45, pp. 70-79.

Richards, T.C. 1961 Motion of the ground on arrival of reflected longitudinal and transverse waves at wide angle reflection distances. Geophysics, 26, pp. 277-295.

Ricker, N. 1953 The form and laws of propagation of seismic wavelets. Geophysics, 18, pp. 10-40.

Stonely, R. 1949 The seismological implications of aeolotropy in continental structure. Monthly Notices of the Royal Astronomical Society, Geophysical Supplement, 5, pp. 222-232.

Vanderstoep, D.M. 1966 Velocity anisotropy measurements in wells. Geophysics, 31, pp. 900-916.

Weatherby, B.B., Born, W.T., and Harding, R.L. 1934 Granite and limestone velocity determinations in Arbuckle Mountains, Oklahoma. Bull. Amer. Assoc. Petr. Geol., 18, pp. 106-118.

White, J.E. and Angona, F.A. 1955 Elastic wave velocities in laminated media. J. Acoustical Soc. of Amer., 27, pp. 310-317.

White, J.E. and Sengbush, R.L. 1953 Velocity determinations in near surface formations. Geophysics, 17, pp. 54-70.

Zisman, W.A. 1933 Young's modulus and Poisson's ratio with reference to geophysical applications. Proc. Nat. Acad. Sci., 19, pp. 653-665.

APPENDIX A

FIGURES

Figure A-1. Theoretical spectral ratios for simple two layer models at various thicknesses (D) but with identical layer velocities. The thicker the model, the closer the spectral peaks approach one another.

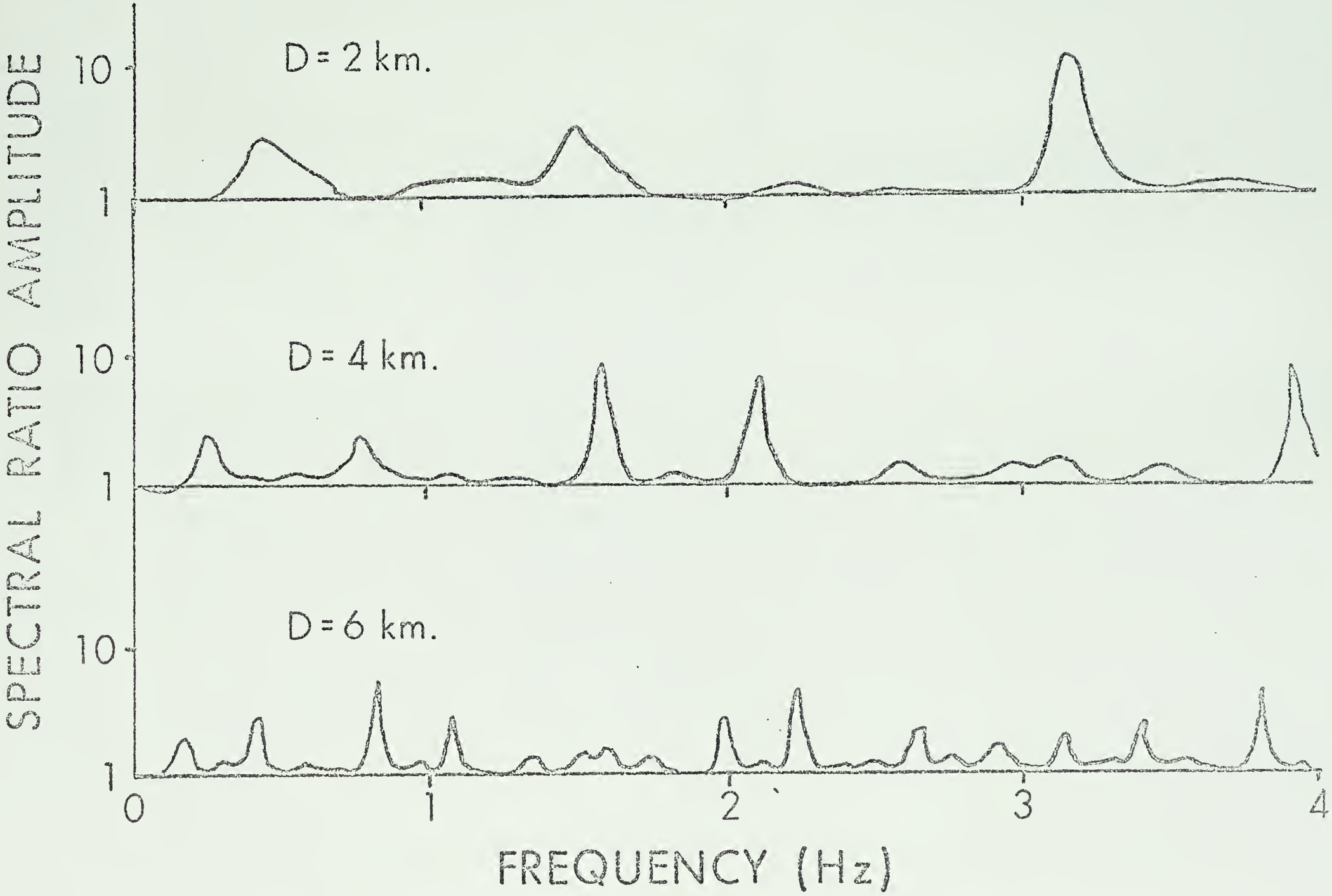
SPECTRAL RATIO AMPLITUDE
D = 2 km.
D = 4 km.
D = 6 km.
10
1
10
1
10
1
0
1
2
3
4
FREQUENCY (Hz)

Figure A-2. Time lag-spectral ratio curve for the OSC events. The OSC3 and OSC4 spectral ratios show peaks at about 12 seconds which corresponds to their pP phase arrival time. OSC2 with a pP time of 6 seconds does not show the distinctive peaks at 12 seconds.

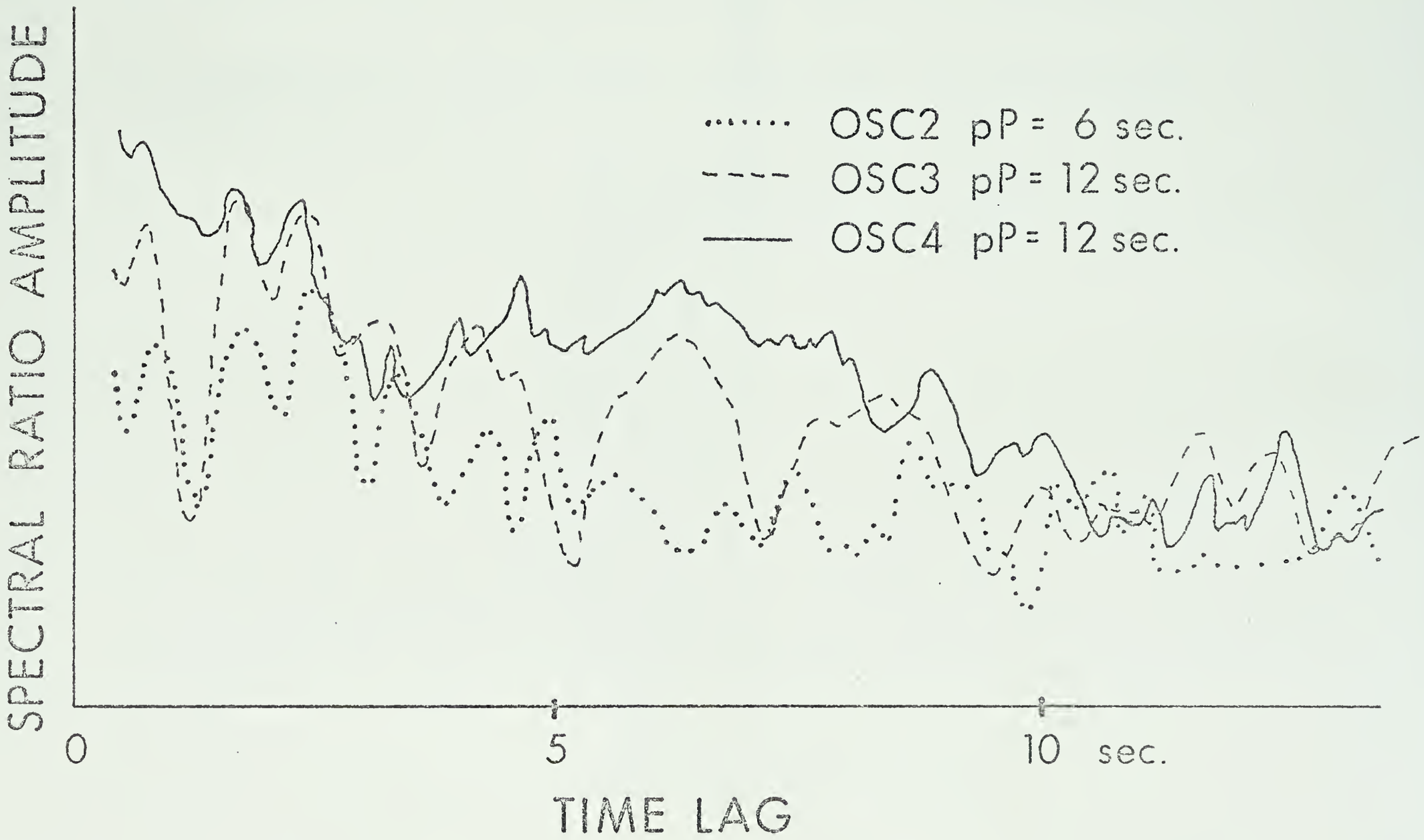
SPECTRAL RATIO AMPLITUDE
OSC2 pP = 6 sec.
OSC3 pP = 12 sec.
OSC4 pP = 12 sec.
0
5
10 sec.
TIME LAG

Figure A-3. Comparison of the spectral ratios for the Oct. 31 event; one with a ten second P-coda window, the other with a forty second window. The forty second window provides considerably more resolution.

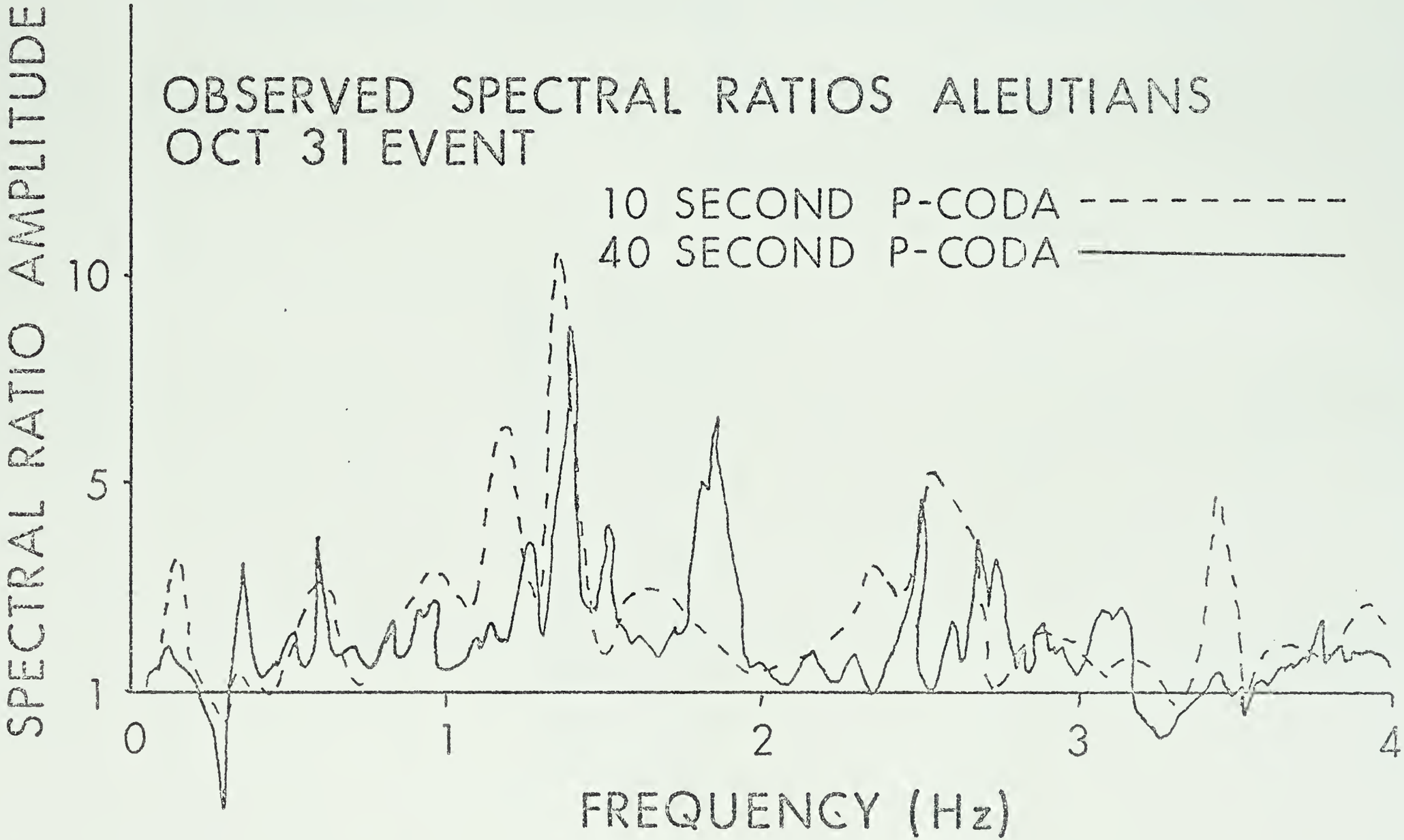
OBSERVED SPECTRAL RATIOS ALEUTIANS
OCT 31 EVENT
10 SECOND P-CODA
40 SECOND P-CODA
SPECTRAL RATIO AMPLITUDE
10
5
1
0
1
2
3
4
FREQUENCY (Hz)

Figures A-4, A-5, A-6. Observed spectral ratios at the OBS, VNG, and OSC stations. The extent to which the observed ratios are alike at each station is a measure of the reliability of the spectral ratio method.

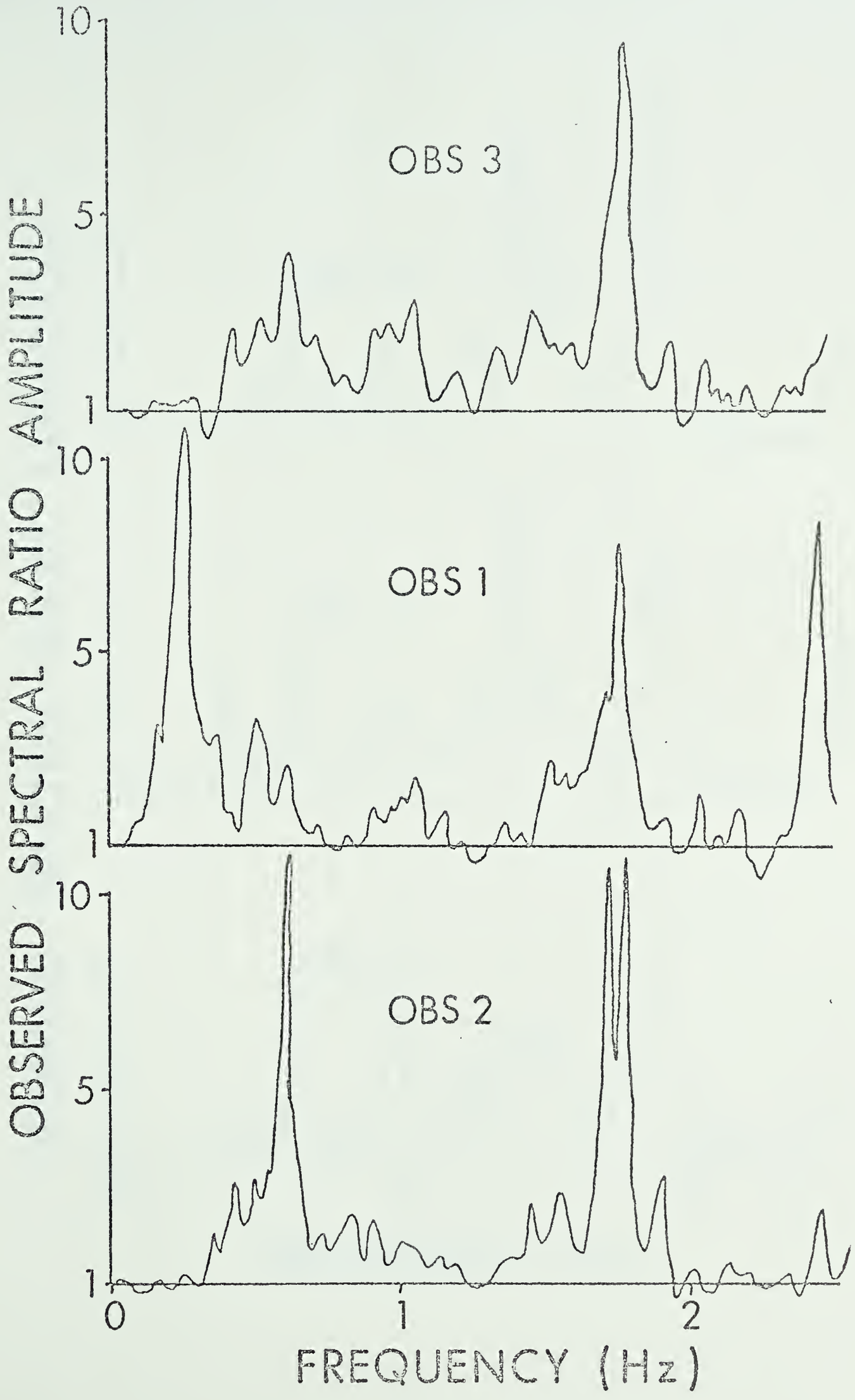
OBSERVED SPECTRAL RATIO AMPLITUDE
10
5
1
OBS 3
10
5
1
OBS 1
10
5
1
OBS 2
0
1
2
FREQUENCY (Hz)

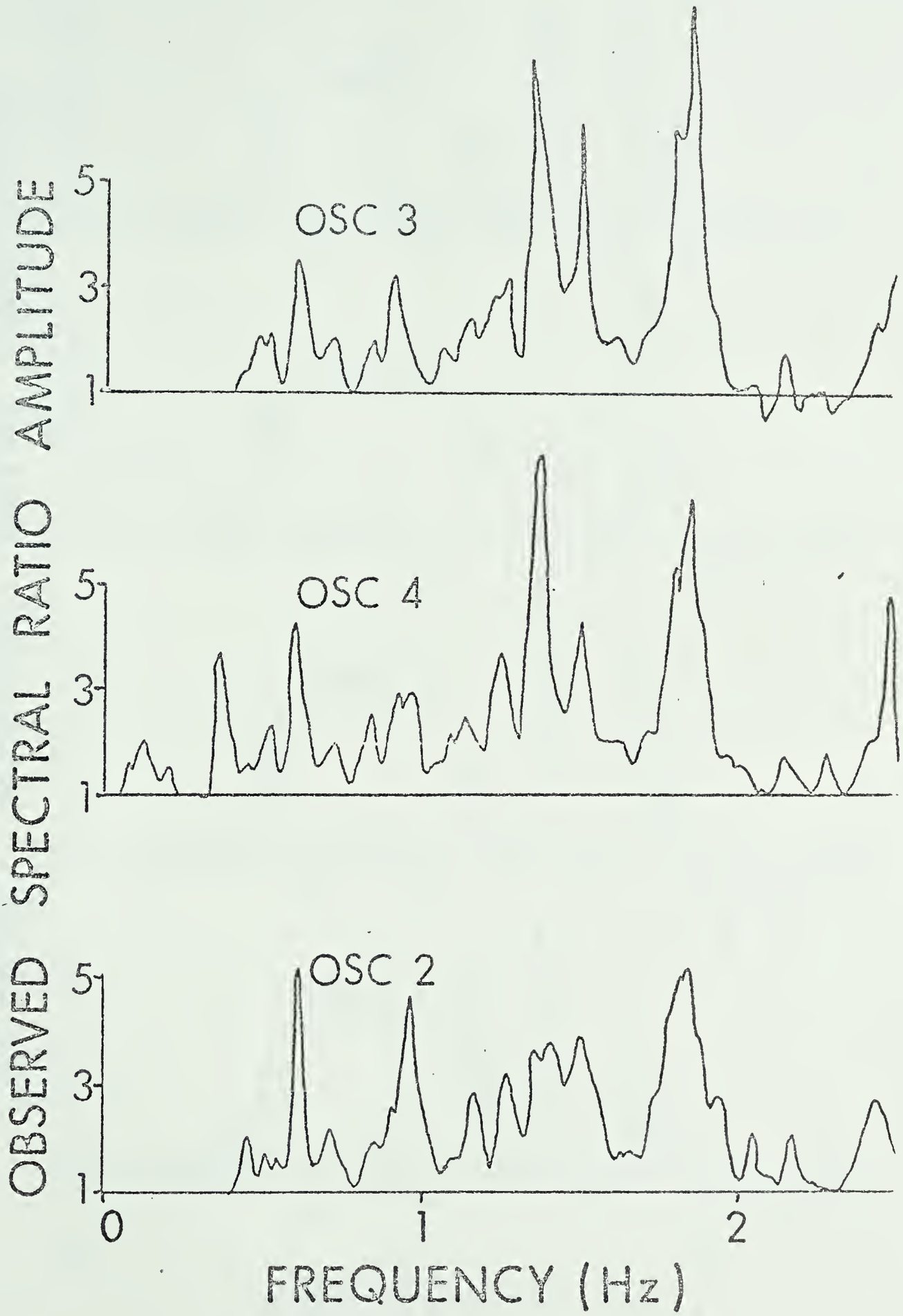
OBSERVED SPECTRAL RATIO AMPLITUDE
OSC 3
OSC 4
OSC 2
5
3
1
0
1
2
FREQUENCY (Hz)

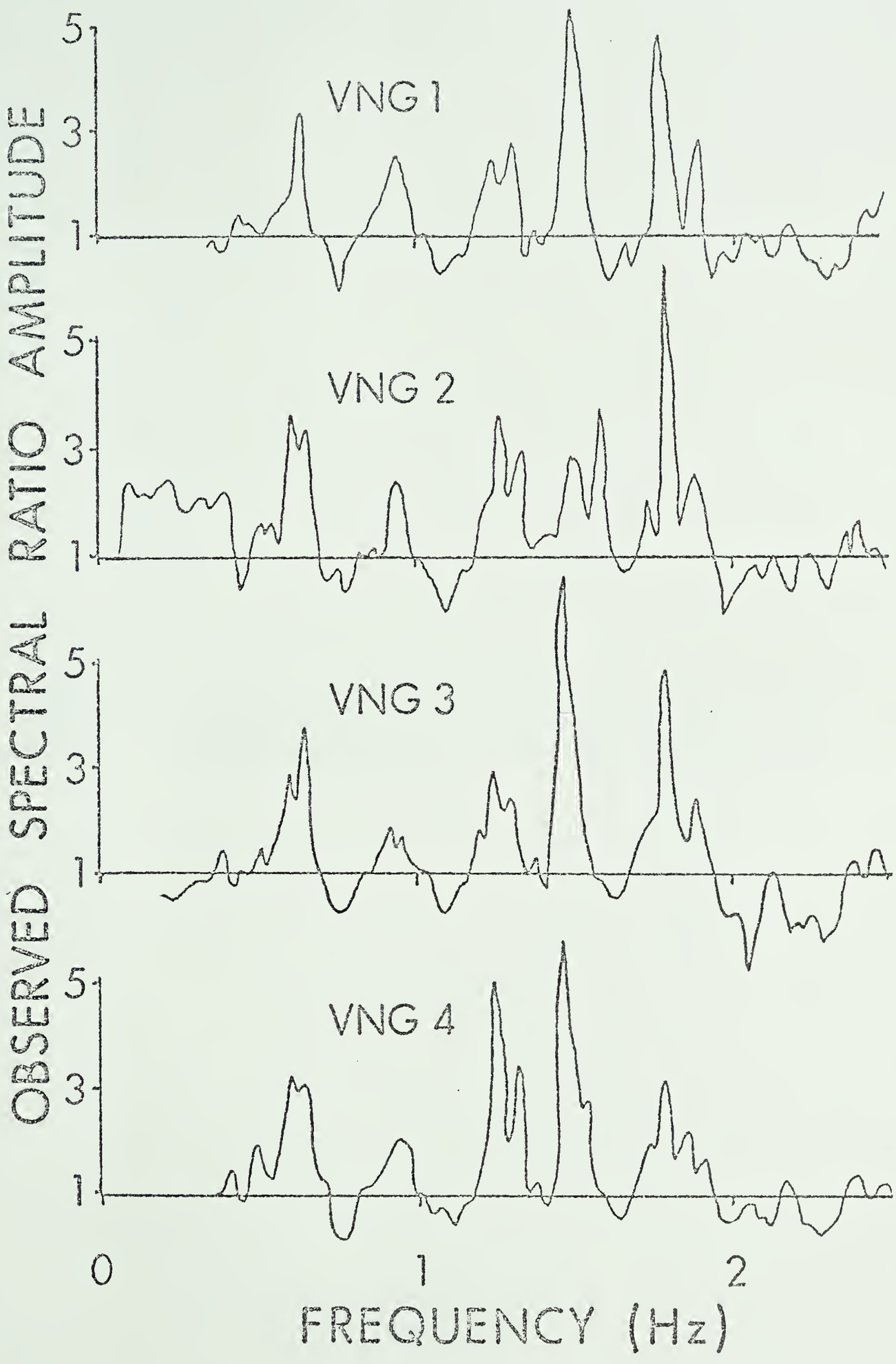
OBSERVED SPECTRAL RATIO AMPLITUDE
VNG 1
VNG 2
VNG 3
VNG 4
5
3
1
0
1
2
FREQUENCY (Hz)

Figure A-7. Comparison of 1969 data at OBS with data collected by other researchers in 1965 and 1968 also at OBS.

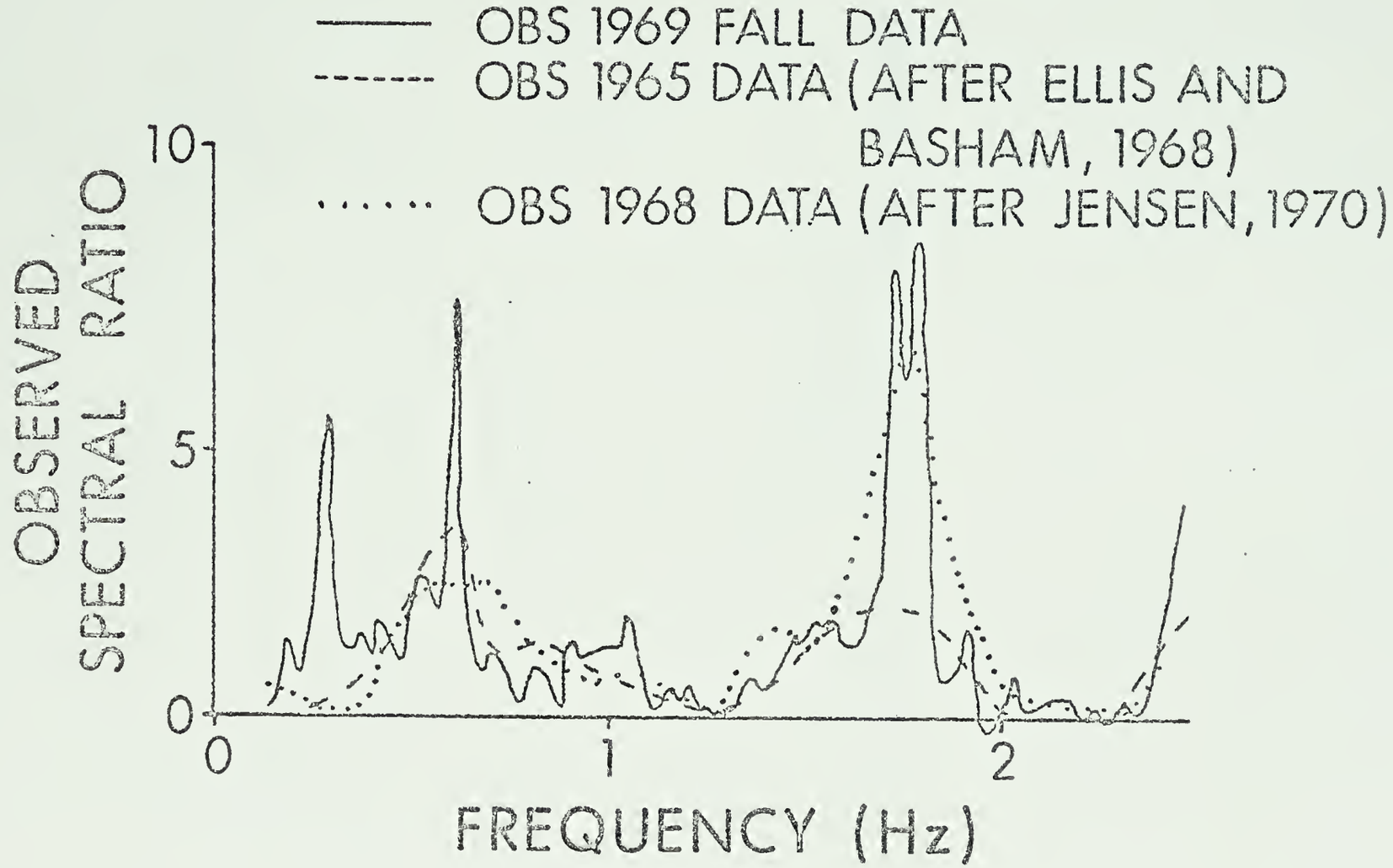
OBS 1969 FALL DATA
OBS 1965 DATA (AFTER ELLIS AND BASHAM, 1968)
OBS 1968 DATA (AFTER JENSEN, 1970)
OBSERVED SPECTRAL RATIO
10
5
0
0
1
2
FREQUENCY (Hz)

Figure A-8. Map showing the area of The University of Alberta's Leduc Observatory.

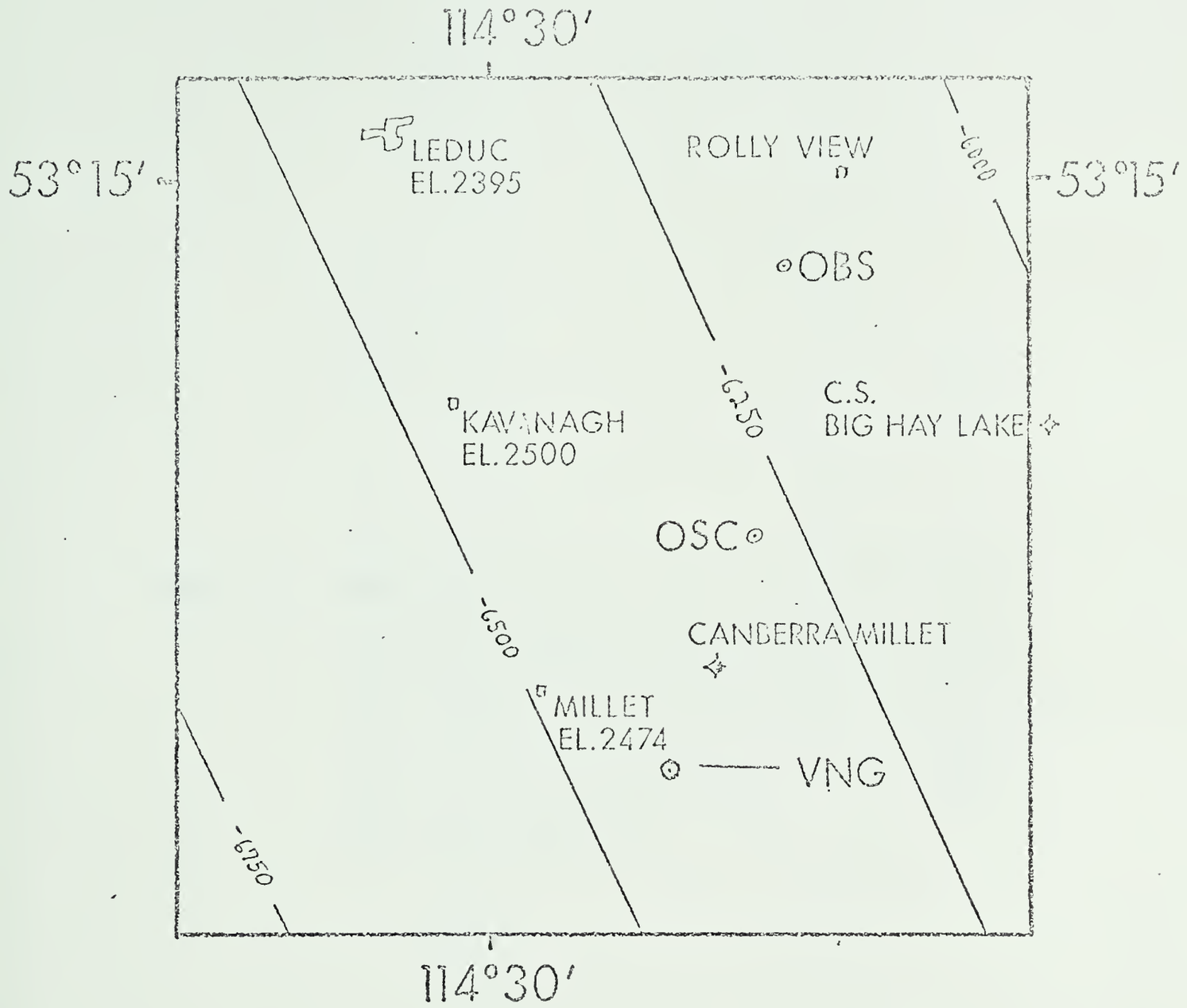

- ⊙ SEISMOGRAPH STATIONS
- ✧ WELLS WITH SONIC LOGS
- ▫ TOWNS
- —— ELEVATION CONTOURS ON BASE OF SEDIMENTS CONTOUR INTERVAL: 250'

LEDUC AREA MAP

0 5 MILES

N

Figure A-9. Theoretical spectral ratios for two nine layer sedimentary models, the only difference between them being the density distribution. The density is seen to affect only the height of the peaks, not their frequency.

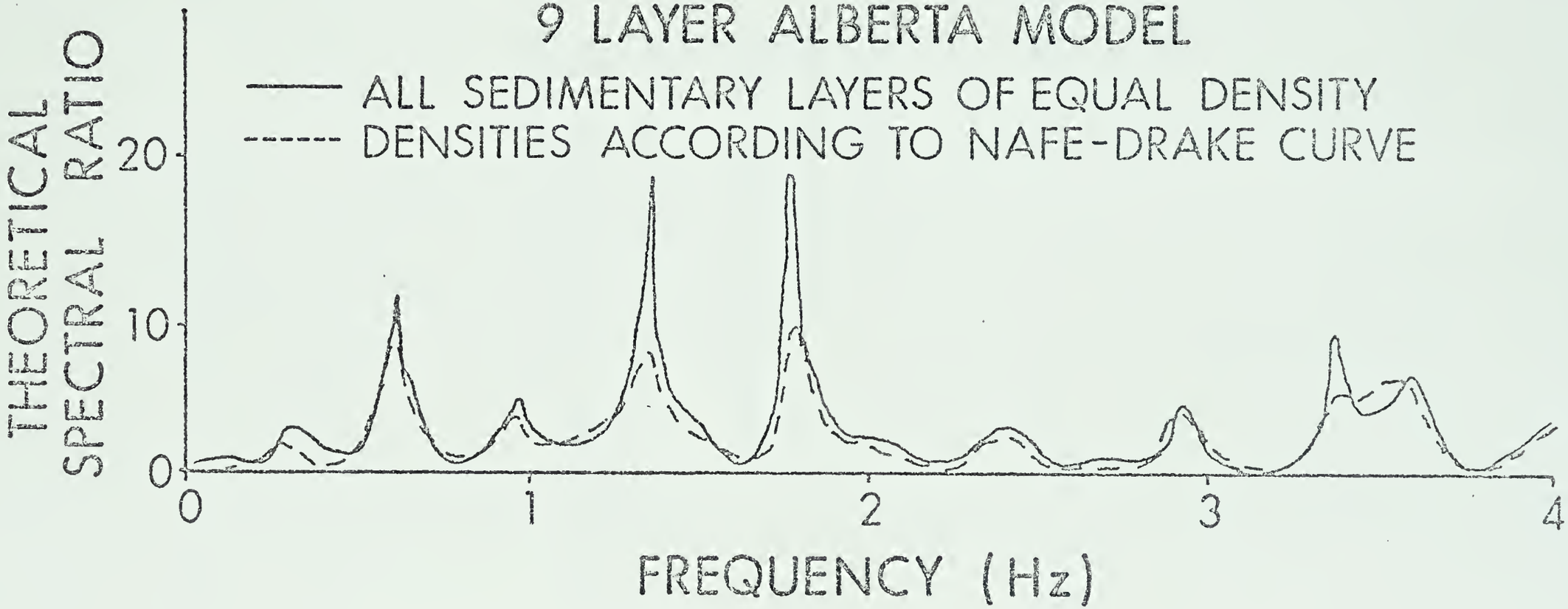
9 LAYER ALBERTA MODEL
ALL SEDIMENTARY LAYERS OF EQUAL DENSITY
DENSITIES ACCORDING TO NAFE-DRAKE CURVE
THEORETICAL SPECTRAL RATIO
20
10
0
0
1
2
3
4
FREQUENCY (Hz)

Figure A-10a. The comparison between the spectral ratios for a seventeen layer model at Leduc and a nine layer model. They are almost identical.

Figure A-10b. The comparison between the seventeen layer model and a three layer model. There are significant differences between the two.

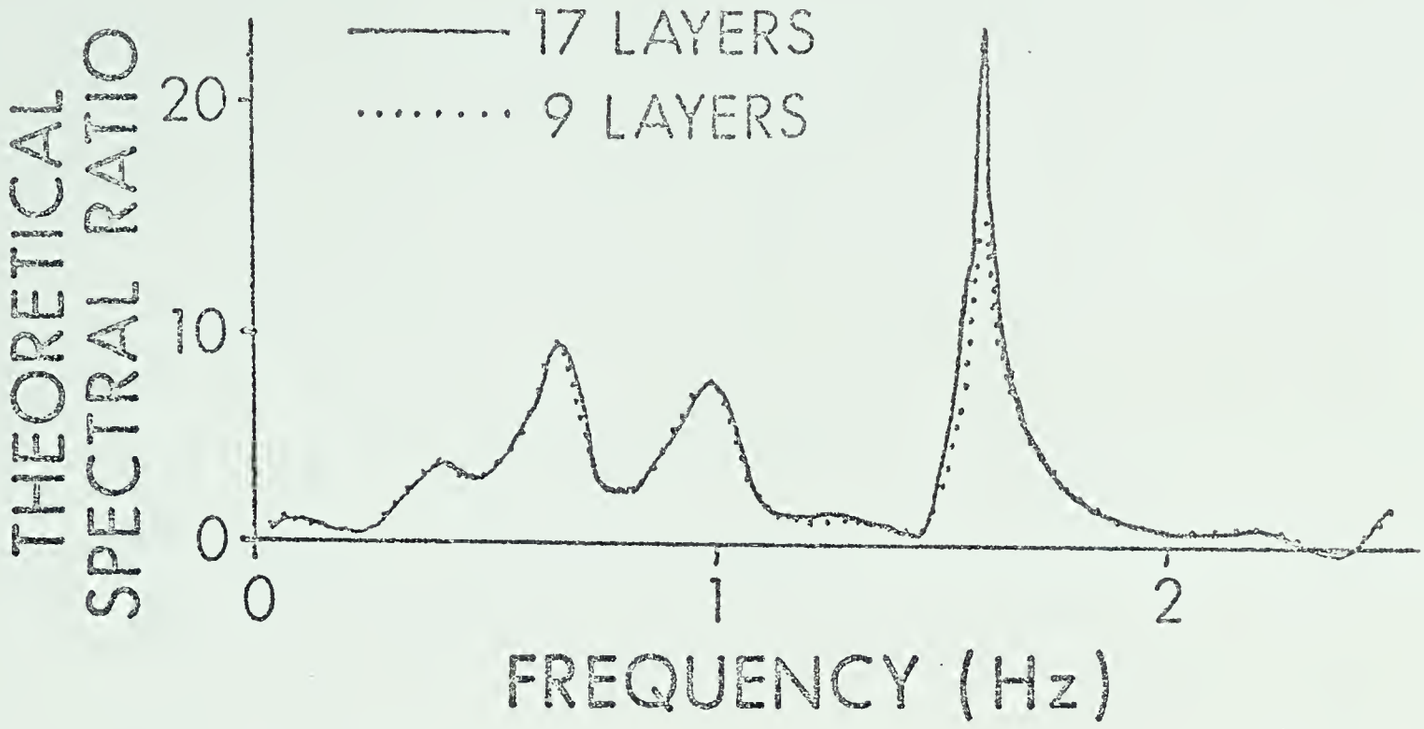
17 LAYERS
9 LAYERS
THEORETICAL SPECTRAL RATIO
20
10
0
0
1
2
FREQUENCY (Hz)

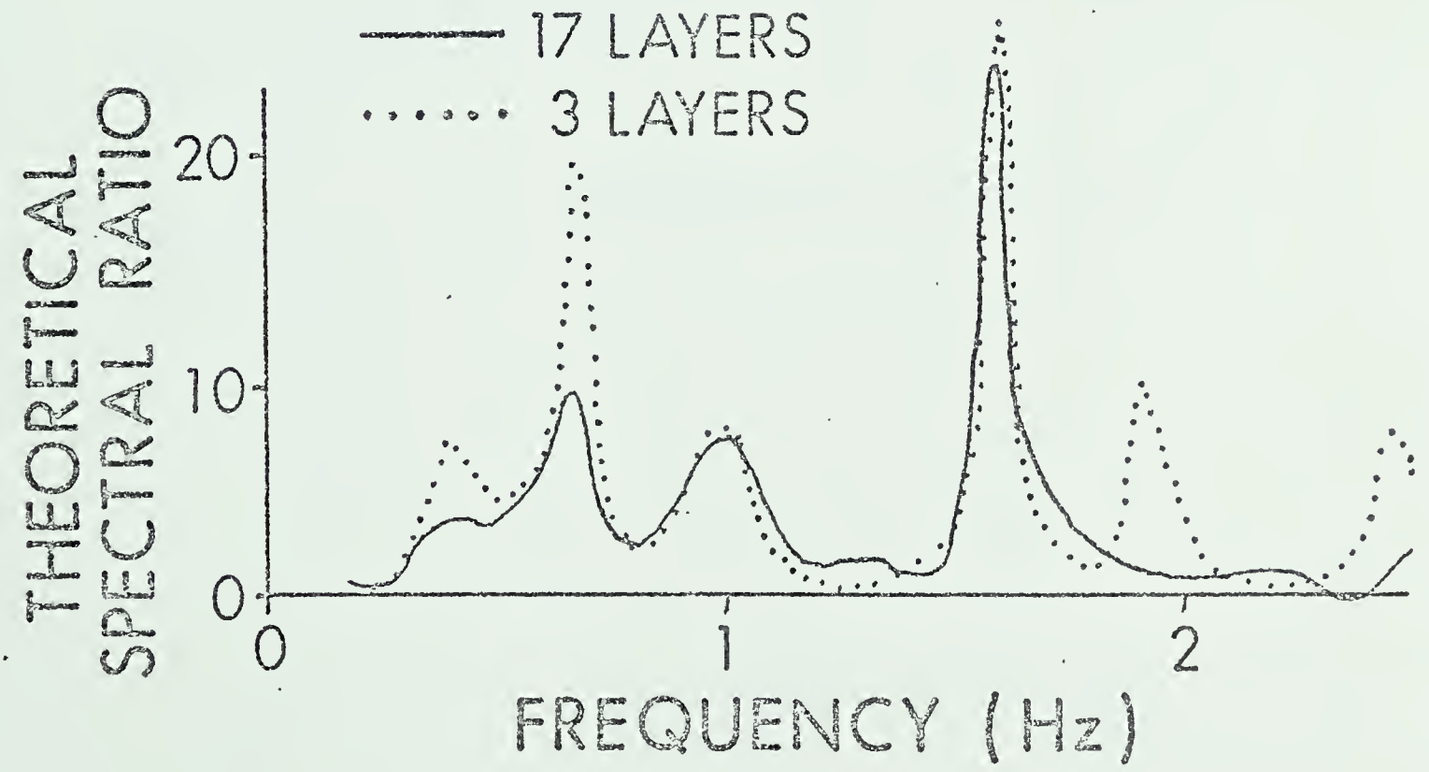
17 LAYERS
3 LAYERS
THEORETICAL SPECTRAL RATIO
20
10
0
0
1
2
FREQUENCY (Hz)

Figure A-11. Comparison between observed and theoretical spectral ratios using a model based only on the sedimentary crustal layers.

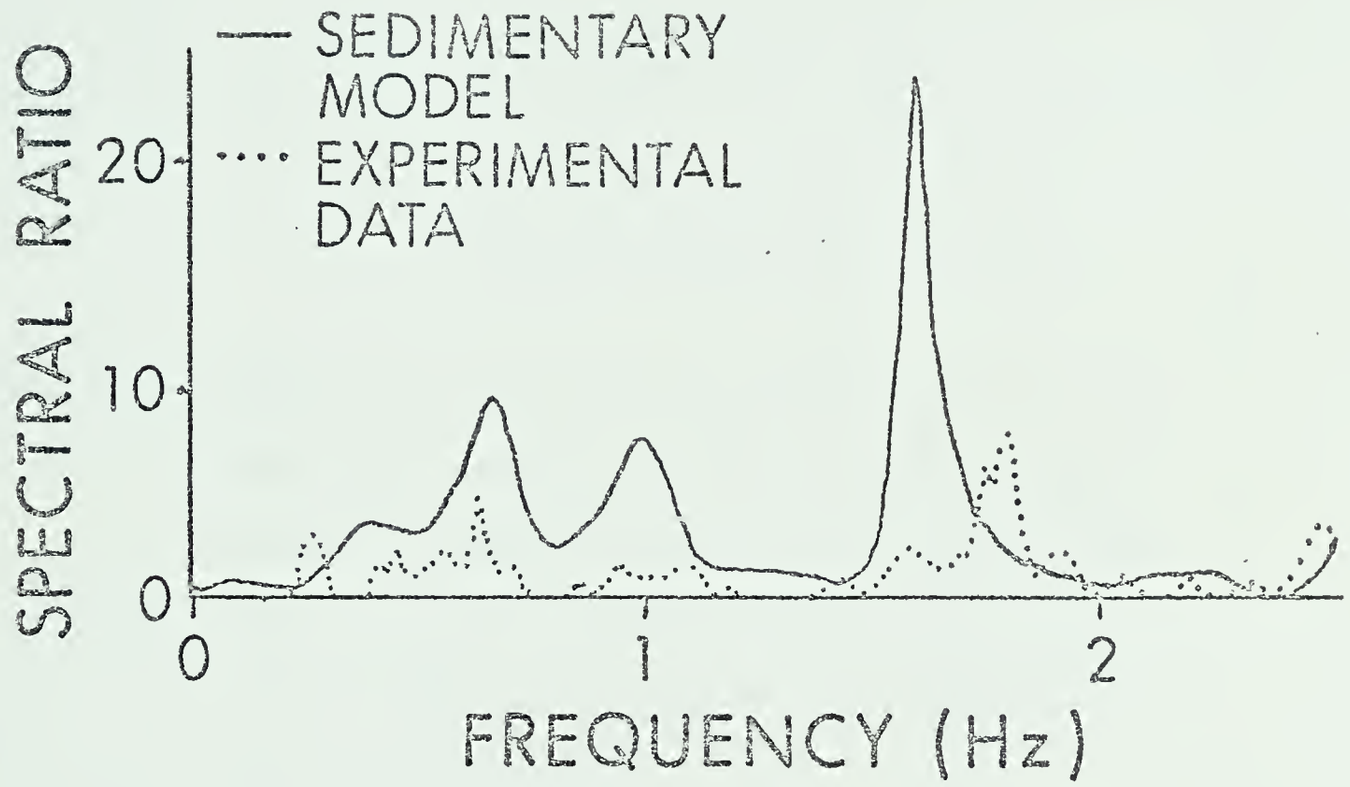
SEDIMENTARY MODEL
EXPERIMENTAL DATA
SPECTRAL RATIO
20
10
0
0
1
2
FREQUENCY (Hz)

Figure A-12. Comparison of the observed spectral ratios at the three field stations. The various peaks do not migrate as predicted from the known geology, hence other factors than simple sedimentary thickening must be affecting the spectral ratios differently at the three stations.

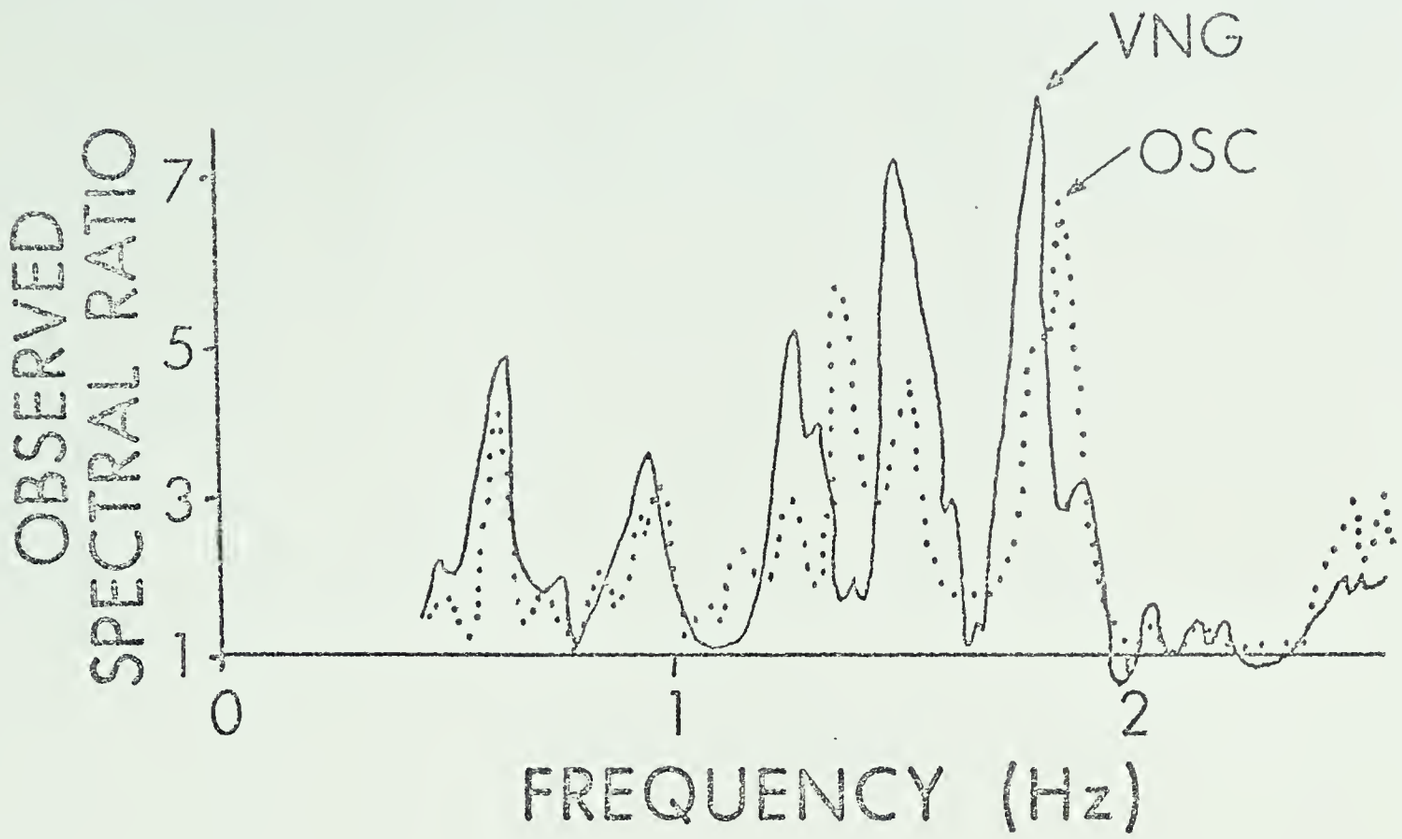
VNG
OSC
OBSERVED
SPECTRAL RATIO
7
5
3
1
0
1
2
FREQUENCY (Hz)

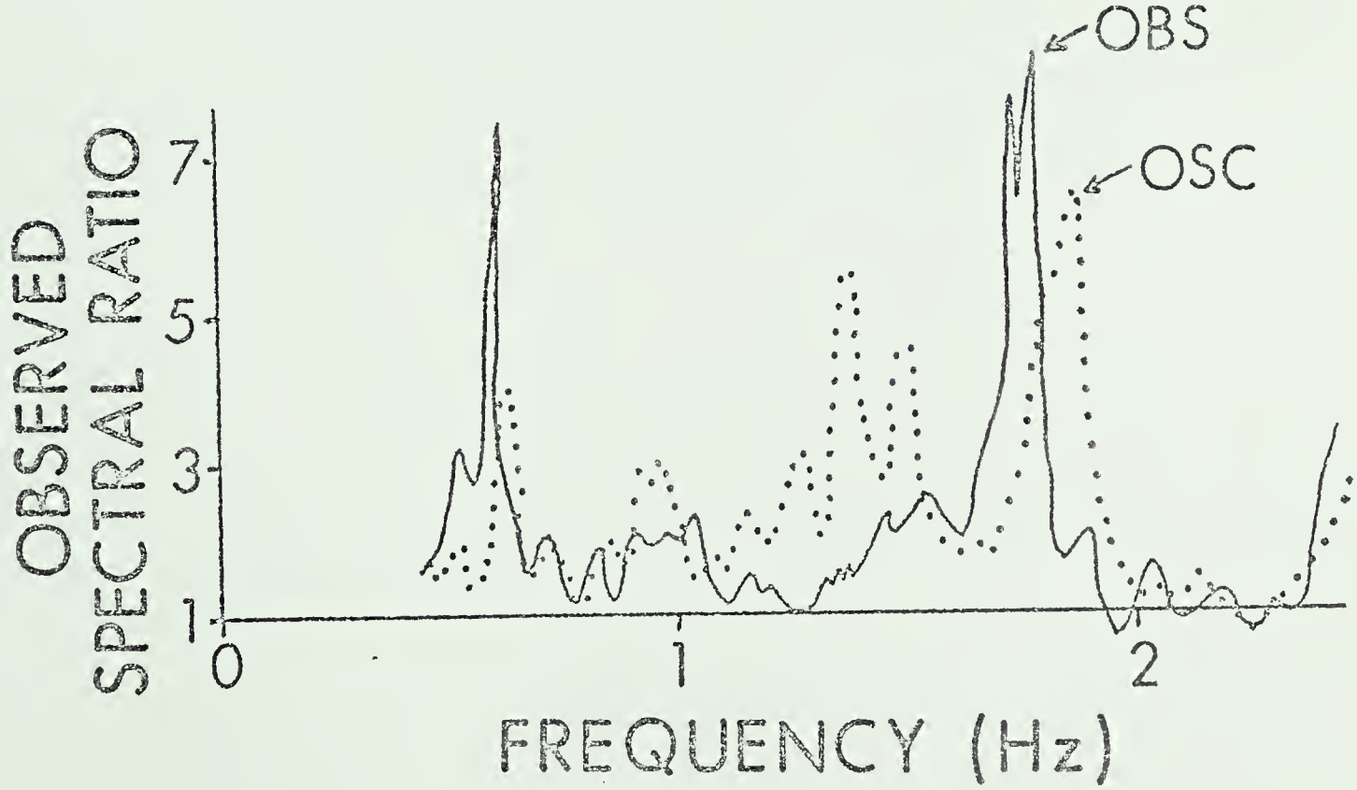
OBS
OSC
OBSERVED
SPECTRAL RATIO
7
5
3
1
0
1
2
FREQUENCY (Hz)

Figure A-13. Theoretical spectral ratios for models with and without the weathering layer.

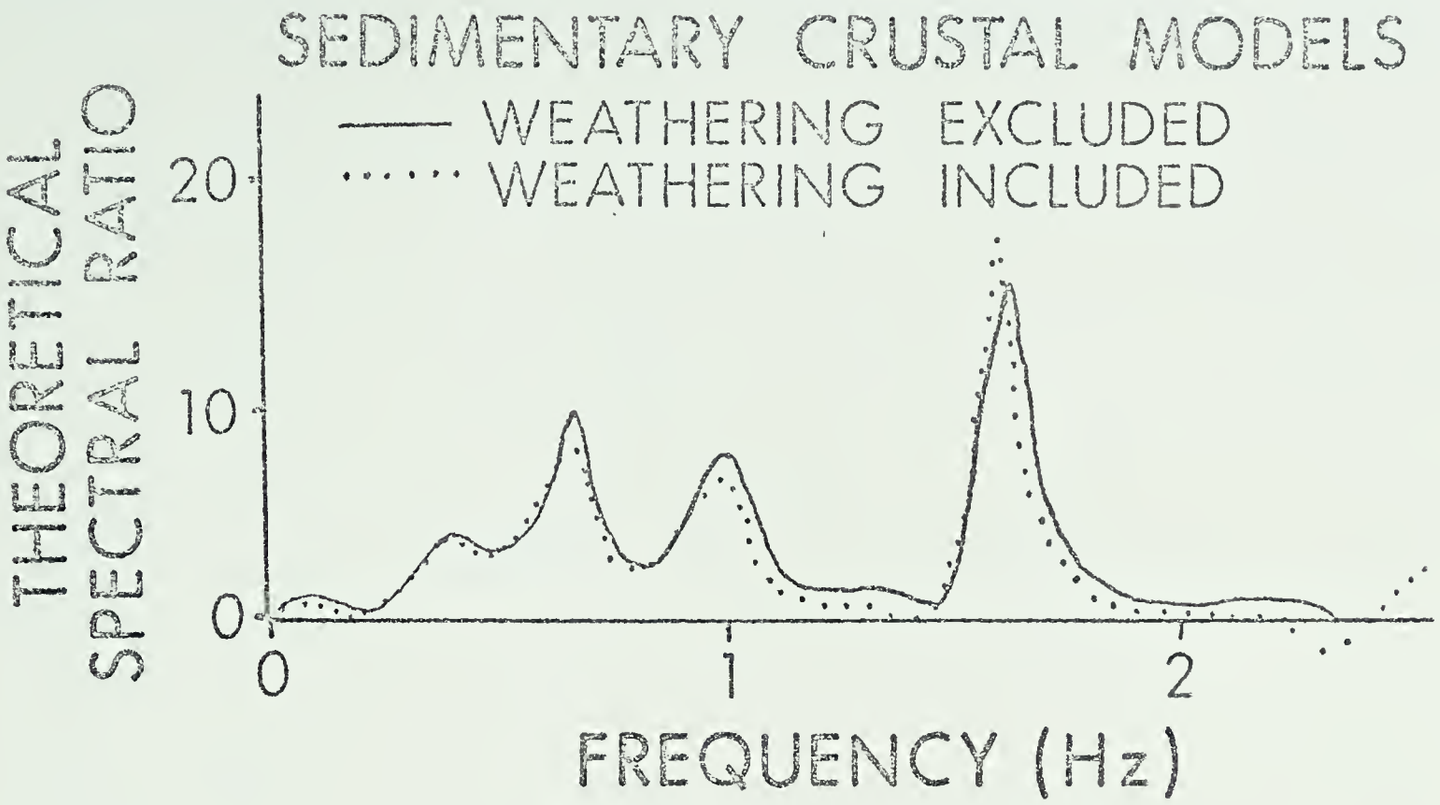
SEDIMENTARY CRUSTAL MODELS
WEATHERING EXCLUDED
WEATHERING INCLUDED
THEORETICAL SPECTRAL RATIO
20
10
0
0
1
2
FREQUENCY (Hz)

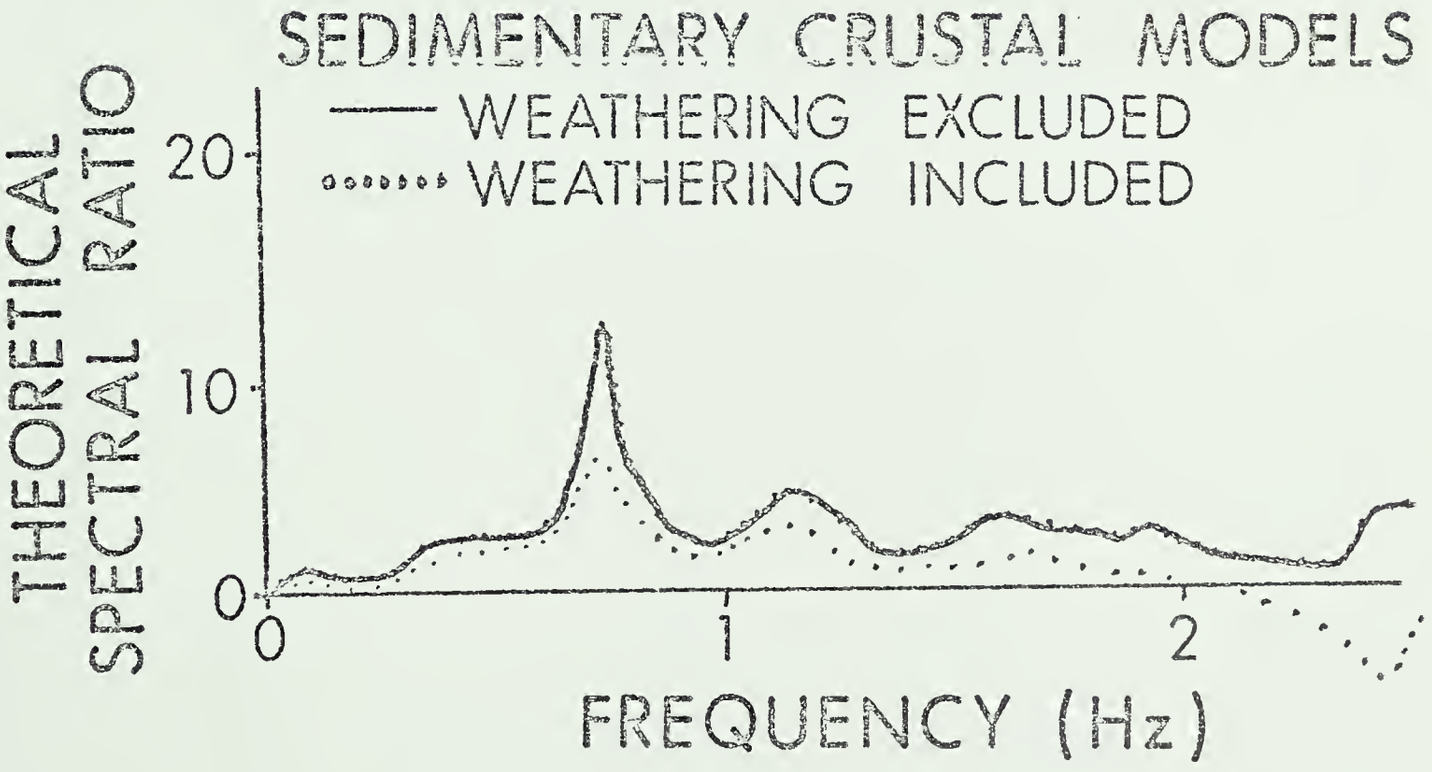
SEDIMENTARY CRUSTAL MODELS
WEATHERING EXCLUDED
WEATHERING INCLUDED
THEORETICAL SPECTRAL RATIO
20
10
0
0
1
2
FREQUENCY (Hz)

Figure A-14. Theoretical spectral ratios for the nine layer Leduc model for values of Poisson's ratio varying from 0.25 to 0.38. Superimposed on each of these is the OBS data.

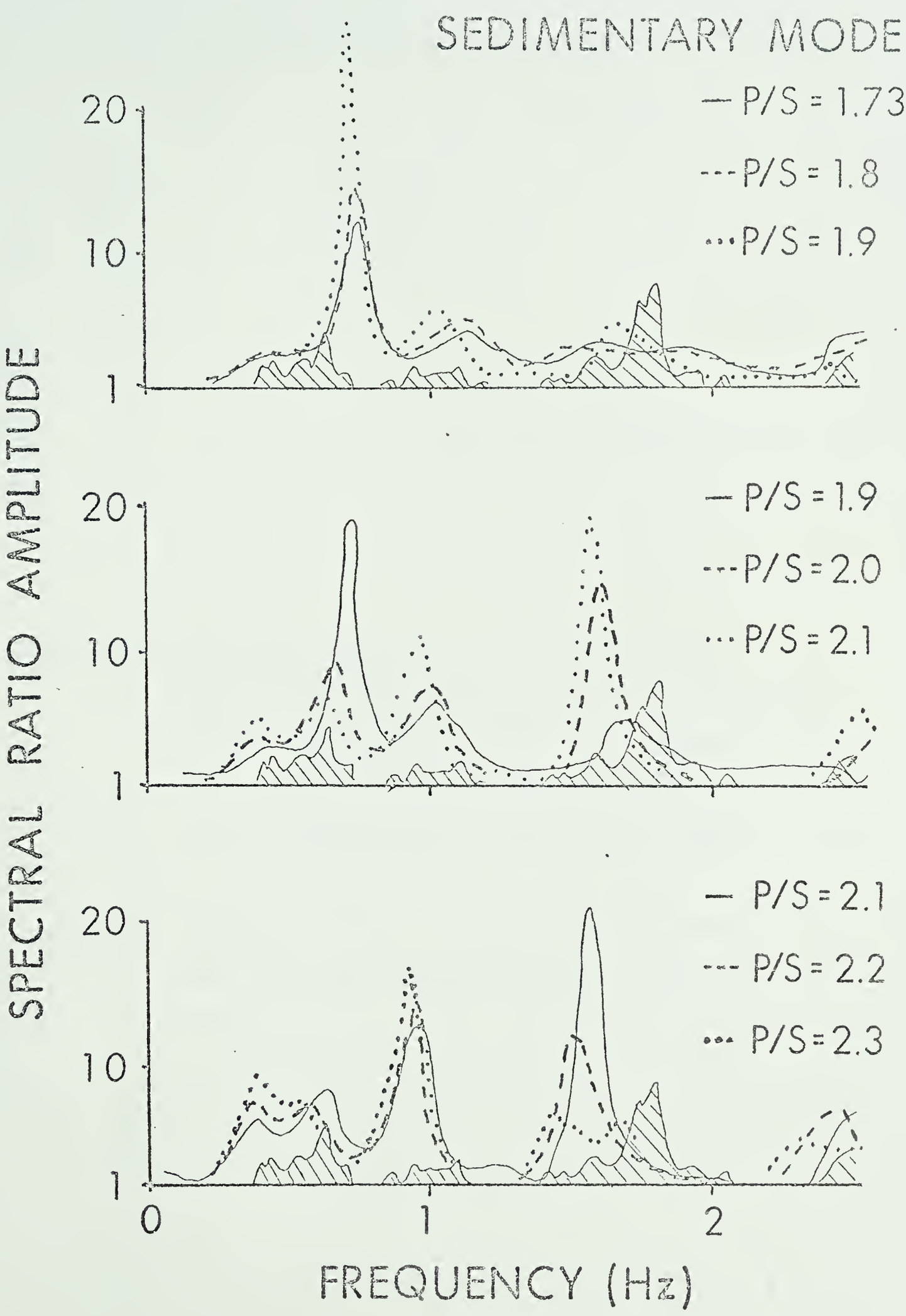
SEDIMENTARY MODELS
— P/S = 1.73
--- P/S = 1.8
··· P/S = 1.9
— P/S = 1.9
--- P/S = 2.0
··· P/S = 2.1
— P/S = 2.1
--- P/S = 2.2
··· P/S = 2.3
SPECTRAL RATIO AMPLITUDE
20
10
1
0
1
2
FREQUENCY (Hz)
▨ - OBSERVED DATA AT OBS.

Figure A-15a. Theoretical spectral ratio for a sedimentary crustal model with a Poisson's ratio of 0.25 in hard layers and 0.33 in soft layers compared with the spectral ratio for the same model with Poisson's ratio equal to 0.33 in all the layers.

Figure A-15b. Comparison of spectral ratios for the isotropic and anisotropic sedimentary crustal models at Leduc.

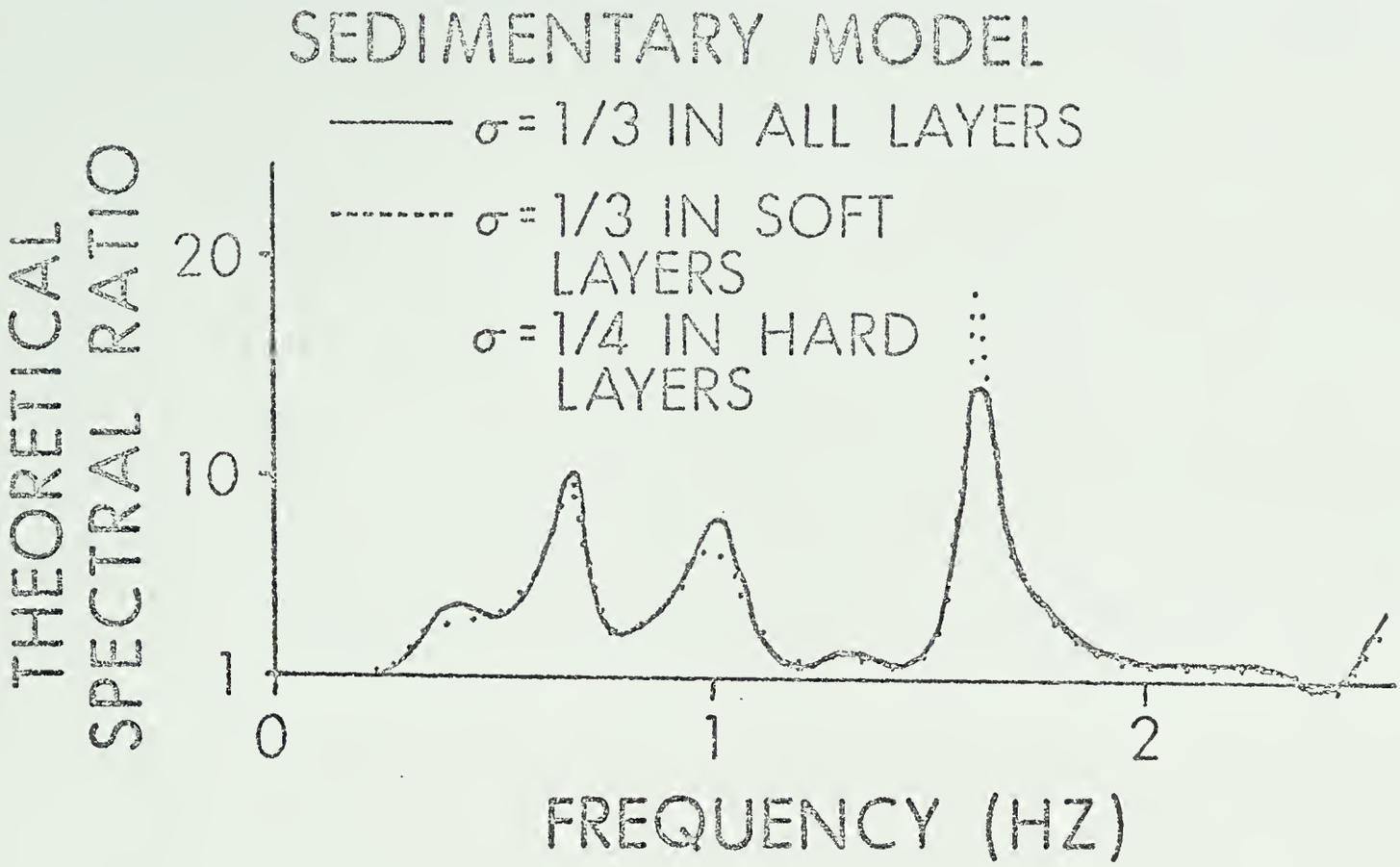
SEDIMENTARY MODEL
σ = 1/3 IN ALL LAYERS
σ = 1/3 IN SOFT LAYERS
σ = 1/4 IN HARD LAYERS
THEORETICAL SPECTRAL RATIO
20
10
1
0
1
2
FREQUENCY (HZ)

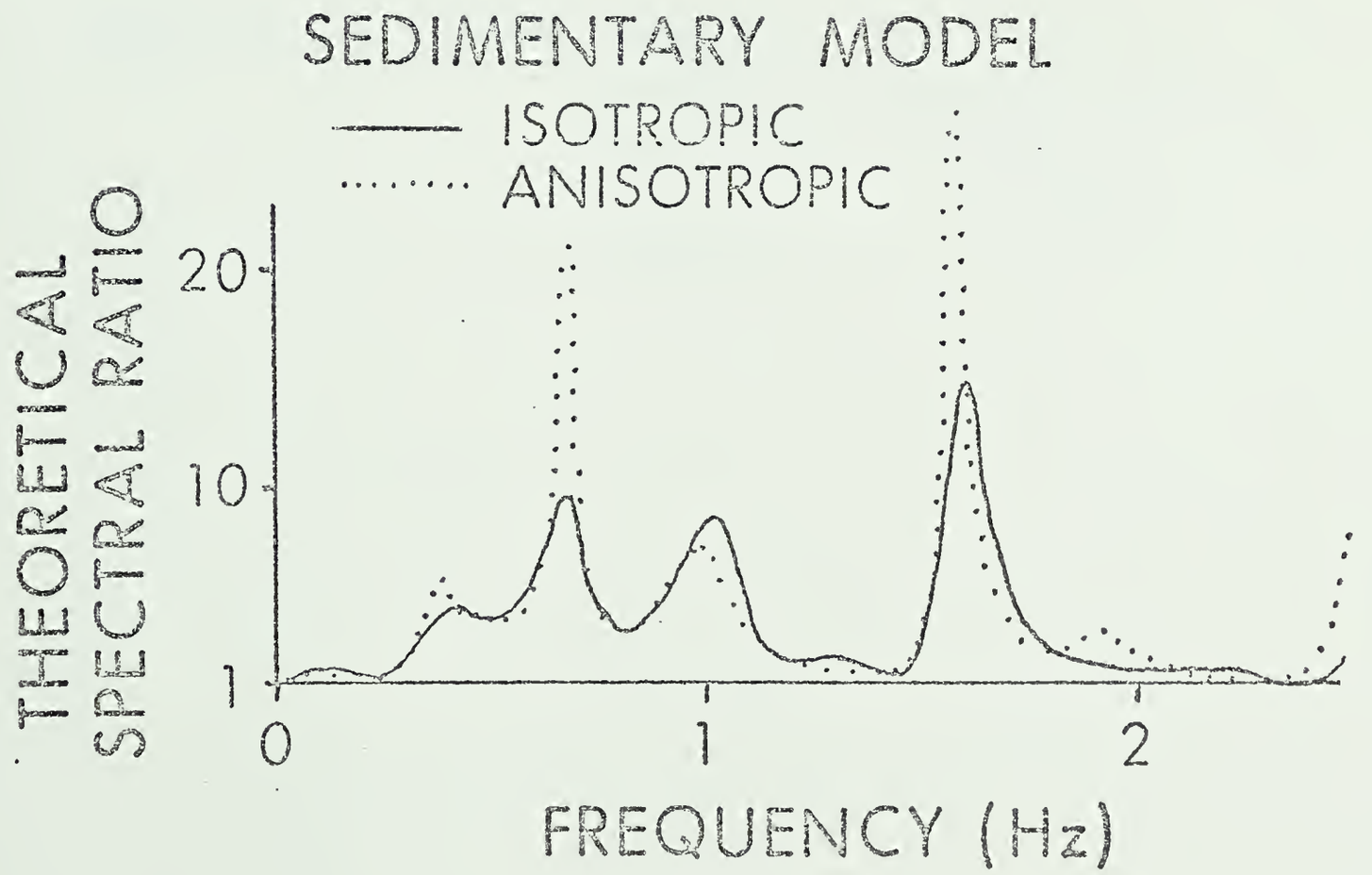
SEDIMENTARY MODEL
ISOTROPIC
ANISOTROPIC
THEORETICAL SPECTRAL RATIO
20
10
1
0
1
2
FREQUENCY (Hz)

Figure A-16a, A-16b, A-16c. Comparison of spectral ratios for isotropic and anisotropic sedimentary crustal models at various angles of incidence.

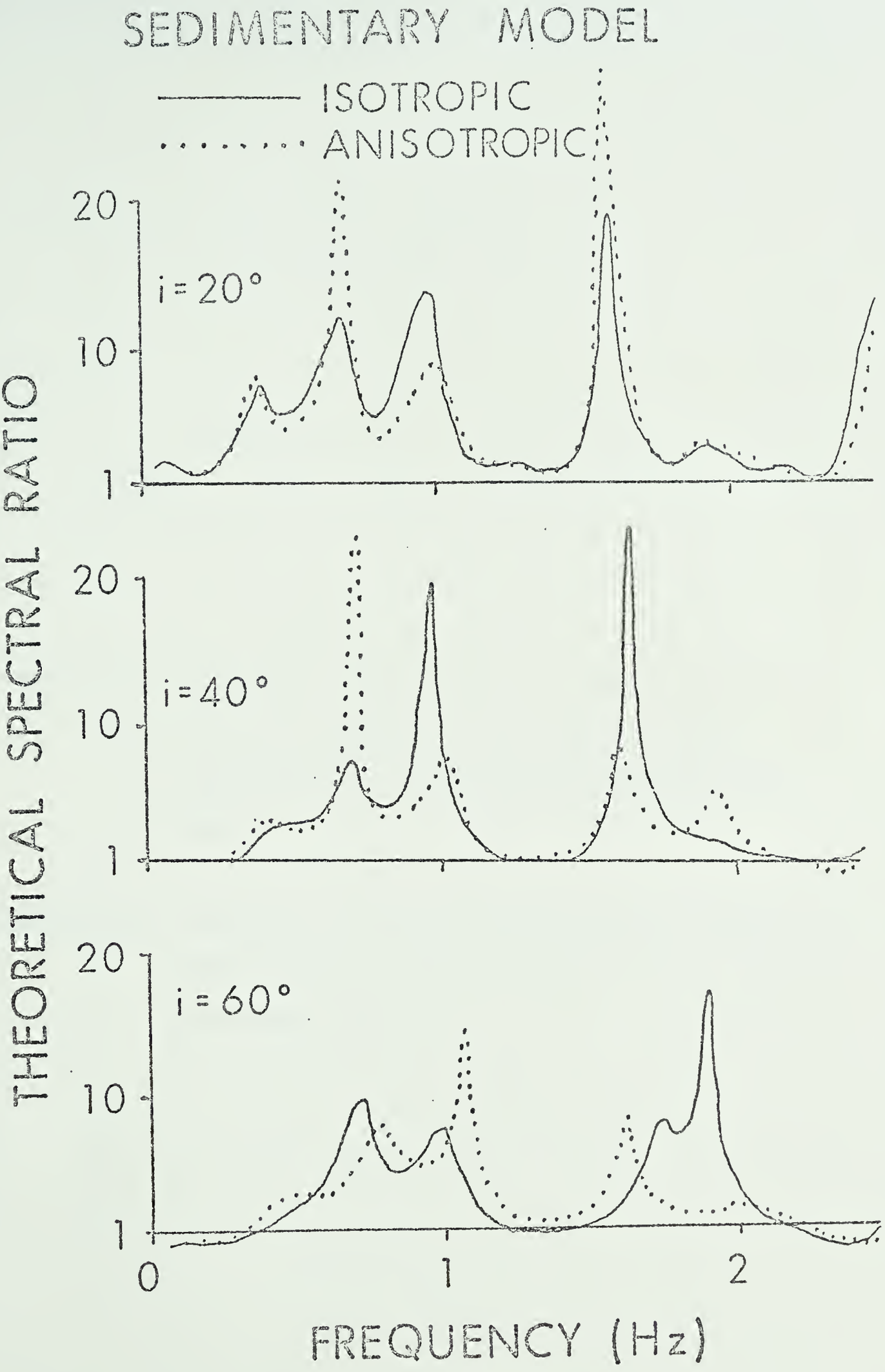
SEDIMENTARY MODEL
ISOTROPIC
ANISOTROPIC
THEORETICAL SPECTRAL RATIO
i = 20°
i = 40°
i = 60°
20
10
1
0
1
2
FREQUENCY (Hz)

Figure A-17a. Theoretical spectral ratios for a model consisting of only the sediments at Leduc and for a model consisting of the sediments plus the deeper crustal layers.

Figure A-17b. Theoretical and observed spectral ratios at station OSC for a model involving a shallow 2000 foot layer beneath the sediments.

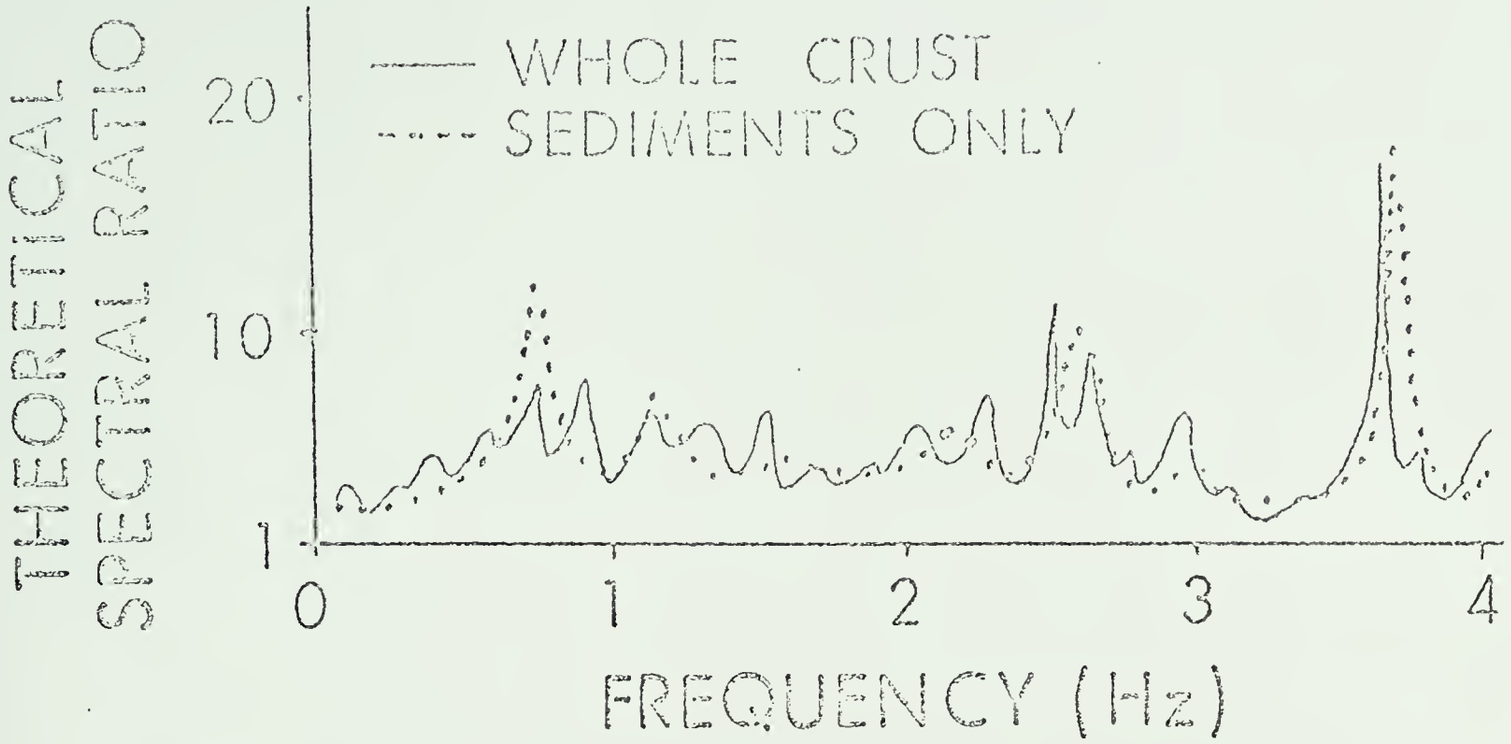
THEORETICAL SPECTRAL RATIO
WHOLE CRUST
SEDIMENTS ONLY
20
10
1
0
1
2
3
4
FREQUENCY (Hz)

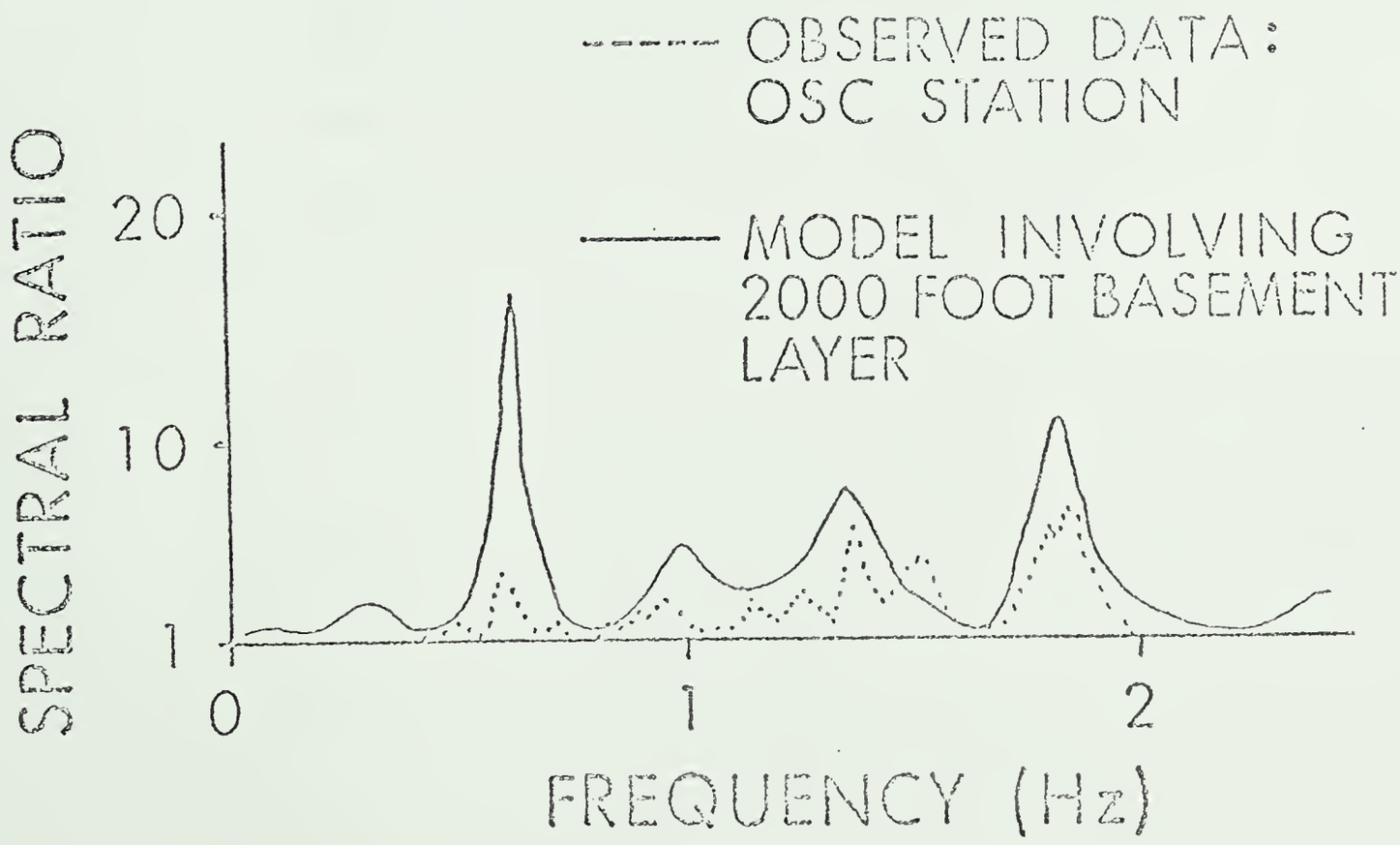
OBSERVED DATA:
OSC STATION
MODEL INVOLVING
2000 FOOT BASEMENT
LAYER
SPECTRAL RATIO
20
10
1
0
1
2
FREQUENCY (Hz)

Figure A-18. Comparison of the observed ratio at OBS with models involving a 3.1 second marker, a 3.1 second marker plus the Conrad discontinuity, and a 3.1 second marker plus both the Conrad and Mohorovicic discontinuities.

Figure A-19a. Observed spectral ratio at VNG station compared with the theoretical spectral ratio for a model involving a 3.0 second marker in the basement.

Figure A-19b. Theoretical spectral ratios for models with a 3.1 second marker but with varying basement velocity.

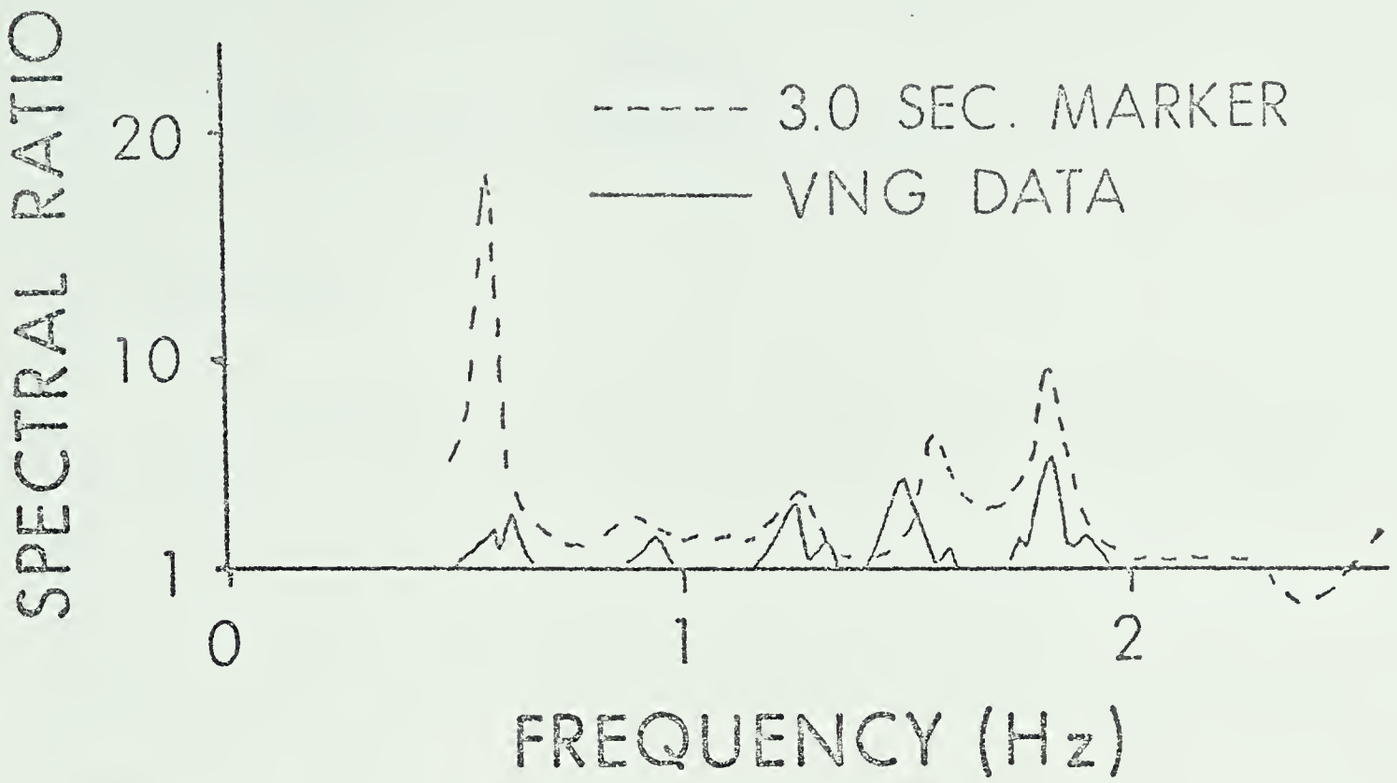
SPECTRAL RATIO
20
10
1
0
1
2
FREQUENCY (Hz)
----- 3.0 SEC. MARKER
—— VNG DATA

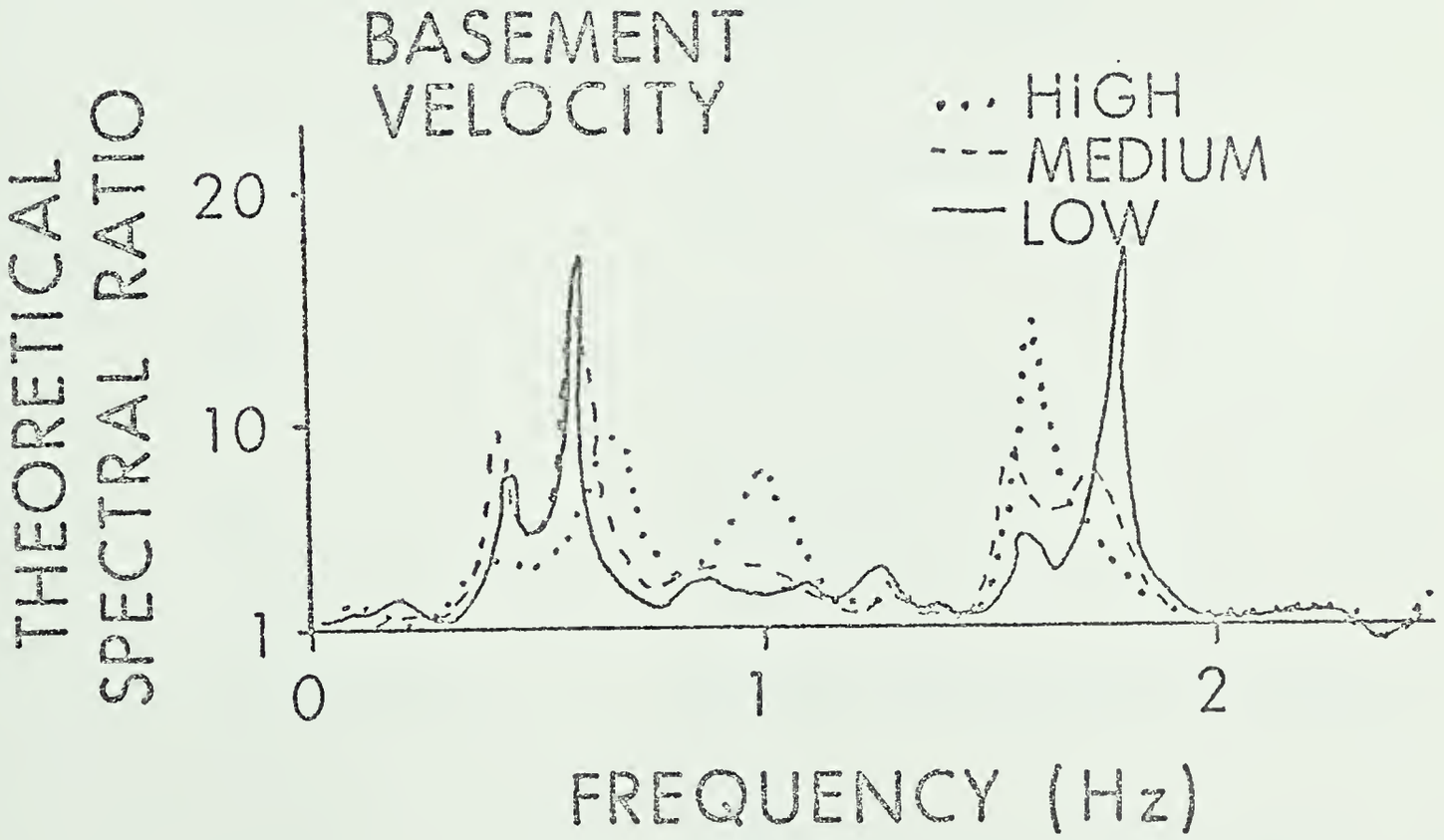
BASEMENT
VELOCITY
THEORETICAL
SPECTRAL RATIO
20
10
1
0
1
2
FREQUENCY (Hz)
··· HIGH
--- MEDIUM
— LOW

APPENDIX B

ELASTIC WAVES IN A TRANSVERSELY ISOTROPIC MEDIA

B.1 Introduction

A mathematical discussion of seismic wave propagation in a transversely isotropic media and the derivation of the matrix formula for the P-coda spectral ratio in a horizontally layered anisotropic system are given in this appendix. Listed below are all the mathematical symbols used in order of appearance as well as a qualitative description of each.

x, y, z, or x_i	Cartesian coordinates
x', y', z'	Transformed coordinates
θ	Angle of rotation
c_{ij}	Matrix of elastic constants
e_{ij}	Strain tensor
W	Strain energy function
P_{ij}	Stress tensor
u_i or u, v, w	Displacement in the i direction
$\dot{u}_i$ or $\dot{u}$, $\dot{v}$, $\dot{w}$	Particle velocity in the i direction
t	Time
l_i, n_i	Direction cosines for type i waves
r_i	Cotangent of angle of incidence
k_i	Wave number for type i waves

c_i	Velocity for type i waves
λ, μ	Lame's Constants
c	Phase velocity along surface
ρ	Density
U_d, W_d	Maximum amplitudes of downgoing wave in the horizontal and vertical directions
ω	Angular frequency
α_v, α_H	P-wave velocity in vertical and horizontal directions
β_v, β_H	S-wave velocity in vertical and horizontal directions
$U_{d\alpha}$, $U_{d\beta}$, $U_{u\alpha}$, $U_{u\beta}$	Maximum amplitude of the downgoing and upgoing "P" and "S" waves respectively
k	Horizontal wave number
P, Q, R, S	Exponential factors for sinusoidal plane waves
$i\gamma_\alpha$, $i\gamma_\beta$	Ratios of vertical and horizontal maximum amplitudes for "P" and "S" waves respectively; functions only of the elastic parameters, density, frequency, and angle of incidence
U_1, U_2, U_3, U_4	Sums and differences of maximum amplitudes of upgoing and downgoing "P" and "S" waves
X_α, X_β, Y_α, Y_β	Stress amplitude factors; functions only of the elastic parameters, density, frequency, and angle of incidence

m, m-1, m-2, etc.	Subscripts indicating layer under analysis as counted from the top of the layered system
D_m	4 x 4 matrix relating the particle velocity and stress vector to the amplitude vector in layer m
$\bar{V}_m$	Particle velocity and stress vector for layer m
E_m	Matrix D_m with z = 0
E_m^{-1}	Inverse of matrix E_m
A_m, B_m	Combinations of stress and displacement amplitude factors; A_m is always imaginary, B_m is always real
a_m	Product of matrices D_m and E_m^{-1} for layer m
n	Number of layers in the system
J	Matrix product for all layers combined
$\bar{U}_m$	Amplitude vector for layer m
D	Determinant of the coefficients from the equations relating J to the boundary conditions of the media
R	P-coda spectral ratio
U_p, W_p	Horizontal and vertical transfer functions

B.2 Equations of Motion

For a transversely isotropic medium with a vertical (z) axis, the following directional and rotational substitutions should not affect the nature of seismic propagation; that is, they should not alter the strain energy function, W,

$$\begin{aligned} x' &= x \\ y' &= y \\ z' &= -z \end{aligned} \qquad \text{B.1}$$

due to symmetry about any horizontal plane, and

$$\begin{aligned} x &= x' \cos\theta - y' \sin\theta \\ y &= x' \sin\theta + y' \cos\theta \\ z &= z' \end{aligned} \qquad \text{B.2}$$

due to symmetry about the vertical axis where the primed symbols are the transformed coordinates and θ is the angle of rotation. Love (1920) performed these substitutions in the strain energy function and determined that twenty-one independent elastic constants are, in fact, reduced to five in a transversely isotropic body. That is,

$$c_{ij} = \begin{vmatrix} c_{11} & c_{12} & c_{13} & 0 & 0 & 0 \\ c_{12} & c_{11} & c_{13} & 0 & 0 & 0 \\ c_{13} & c_{13} & c_{33} & 0 & 0 & 0 \\ 0 & 0 & 0 & c_{44} & 0 & 0 \\ 0 & 0 & 0 & 0 & c_{44} & 0 \\ 0 & 0 & 0 & 0 & 0 & c_{66} \end{vmatrix} \qquad \text{B.3}$$

where $c_{66} = \frac{c_{11} - c_{12}}{2}$

The strain energy function for a transversely isotropic medium reduces to the following:

$$\begin{aligned} W = 1/2 \{ & c_{11} (e_{xx}^2 + e_{yy}^2) + c_{33} e_{zz}^2 \\ & + 2c_{13} (e_{xx} + e_{yy}) e_{zz} + 2c_{12} e_{xx} e_{yy} \\ & + c_{44} (e_{yz}^2 + e_{zx}^2) + 1/2 (c_{11} - c_{12}) e_{xy}^2 \} \end{aligned} \qquad \text{B.4}$$

where e_{ij} is the strain tensor.

The stresses are then:

$$P_{xx} = \frac{\partial W}{\partial e_{xx}} = c_{11} e_{xx} + c_{12} e_{yy} + c_{13} e_{zz}$$

$$P_{zz} = \frac{\partial W}{\partial e_{zz}} = c_{13} (e_{xx} + e_{yy}) + c_{33} e_{zz}$$

$$P_{yy} = \frac{\partial W}{\partial e_{yy}} = c_{11} e_{yy} + c_{13} e_{zz} + c_{12} e_{xx}$$

$$P_{xy} = \frac{\partial W}{\partial e_{xy}} = (c_{11} - c_{12}) e_{xy}$$

$$P_{yz} = \frac{\partial W}{\partial e_{yz}} = c_{44} e_{yz}$$

$$P_{zx} = \frac{\partial W}{\partial e_{zx}} = c_{44} e_{zx} \qquad \text{B.5}$$

The equations of motion are given by:

$$\rho \frac{\partial^2 u_i}{\partial t^2} = \frac{\partial P_{ij}}{\partial x_j} \qquad \text{B.6}$$

B.3 Derivation of Velocities in a Transversely Isotropic Medium

In order to simplify the problem to a two dimensional case, motion will only be allowed in the x-z plane. SH waves are, therefore, excluded, the displacement in the y direction is zero, all derivatives with respect to y are zero, and the equations of motion become:

$$\rho \frac{\partial^2 u}{\partial t^2} = \frac{\partial P_{xy}}{\partial x} + \frac{\partial P_{xz}}{\partial z}$$

$$\rho \frac{\partial^2 w}{\partial t^2} = \frac{\partial P_{zx}}{\partial x} + \frac{\partial P_{zz}}{\partial z} \qquad \text{B.7}$$

To introduce the anisotropic condition, equations B.5 are substituted in the equations of motion as follows:

$$\rho \frac{\partial^2 u}{\partial t^2} = \frac{\partial}{\partial x} \left(c_{11} \frac{\partial u}{\partial x} + c_{13} \frac{\partial w}{\partial z} \right) + \frac{\partial \left\{ c_{44} \left(\frac{\partial w}{\partial x} + \frac{\partial u}{\partial z} \right) \right\}}{\partial z}$$

$$\rho \frac{\partial^2 w}{\partial t^2} = \frac{\partial}{\partial x} \left\{ \left(c_{44} \left(\frac{\partial u}{\partial z} + \frac{\partial w}{\partial x} \right) \right\} + \frac{\partial}{\partial z} \left(c_{13} \frac{\partial u}{\partial x} + c_{33} \frac{\partial w}{\partial z} \right) \right.$$

B.8

Suitable trial solutions for downgoing plane waves with harmonic time dependence will be of the form

$$u = U_d \cdot \exp \left(iwt - i k_i \left(l_i x + n_i z \right) \right)$$

$$w = -W_d \cdot \exp \left(iwt - ik_i \left(l_i x + n_i z \right) \right) \qquad \text{B.9}$$

where l_i and n_i and k_i are the direction cosines and the wavenumber for waves of type i.

Substituting this trial solution B.9 in the equations of motion, B.8, gives a new equation of motion which may be written in matrix form as

$$\begin{vmatrix} \{l_i^2 c_{11} + n_i^2 c_{44} - \rho c_i^2\} & -l_i n_i (c_{44} + c_{13}) \\ l_i n_i (c_{44} + c_{13}) & -\{l_i^2 c_{44} + n_i^2 c_{33} - \rho c_i^2\} \end{vmatrix} \begin{vmatrix} U_d \\ W_d \end{vmatrix} = 0$$

B.10

where c_i is the velocity for waves of type i.

The velocities of wave propagation can be determined by solving for the two roots in c_i^2 by setting the determinant of the coefficients in equation B.10 equal to zero.

$$\{l_i^2 c_{11} + n_i^2 c_{44} - \rho c_i^2\} \{l_i^2 c_{44} + n_i^2 c_{33} - \rho c_i^2\} - l_i^2 n_i^2 (c_{13} + c_{44})^2 = 0$$

B.11

For vertical rays $l_i = 0$, $n_i = 1$, or

$$\alpha_v = \frac{c_{33}}{\rho} = \text{Vertical P velocity}$$

$$\beta_v = \frac{c_{44}}{\rho} = \text{Vertical S velocity}$$

For horizontal rays, $l_i = 1$, $n_i = 0$, or

$$\alpha_H = \frac{c_{11}}{\rho} = \text{Horizontal P velocity}$$

$$\beta_v = \frac{c_{44}}{\rho} = \text{Horizontal SV velocity}$$

and in a three dimensional case:

$$\beta_H = \frac{c_{11} - c_{12}}{\rho} = \text{Horizontal SH velocity} \qquad \text{B.12}$$

For a wave in any arbitrary direction

$$c_i^2 = \frac{1}{2\rho}\left[c_{11}l_i^2 + c_{33}n_i^2 + c_{44} \pm \left[\{ (c_{11} - c_{44})\, l_i^2 - (c_{33} - c_{44})\, n_i^2 \}^2 + 4 (c_{13} + c_{44})^2 l_i^2 n_i^2\right]^{1/2}\right] \qquad \text{B.13}$$

Both solutions of this equation are real and positive. If the three dimensional case were being considered, another wave would exist as follows, shown by Stonely (1949).

$$c_3^2 = \frac{1}{\rho}\{ l_i^2 \left(\frac{c_{11} - c_{12}}{2}\right) + n_i^2 c_{44} \} \qquad \text{B.14}$$

Hence there are three different velocities to be found for a wave propagating in any direction.

To identify these waves, it is useful to consider the special case of the purely isotropic medium in which

$$c_{11} = c_{33} = \lambda + 2\mu$$

$$c_{13} = c_{12}$$

$$c_{44} = \frac{c_{11} - c_{12}}{2} = \mu \qquad \text{B.15}$$

where λ and μ are Lame's Constants.

The solutions of equation B.13 and B.14 then yield:

$$c_1^2 = \frac{\lambda + 2\mu}{\rho} \quad \text{or a P wave} \qquad \text{B.16}$$

$$c_2^2 = \frac{\mu}{\rho} \quad \text{or a SV wave} \qquad \text{B.17}$$

$$c_3^2 = \frac{\mu}{\rho} \quad \text{or a SH wave} \qquad \text{B.18}$$

Thus in a transversely isotropic body, SV and SH waves generally travel at different velocities.

B.4 Theoretical Spectral Ratios for P-Waves in a System of Horizontal Transversely Isotropic Layers

A solution to the elastic wave equation valid for a transvesely isotropic layer containing both upward and downgoing waves is as following:

$$u = \{U_{d\alpha}e^{-iP} + U_{u\alpha}e^{iP}\} \; e^{R} + \{ U_{d\beta}e^{-iQ} + U_{u\beta}e^{iQ} \} \; e^{S}$$

$$w = -i\gamma_\alpha \{ U_{d\alpha} e^{-iP} - U_{u\alpha} e^{iP} \} e^{R} - i\gamma_\beta \{ U_{d\beta} e^{-iQ} - U_{u\alpha} e^{iQ} \} e^{S}$$

B.19

where: $U_{d\alpha}$, $U_{d\beta}$, $U_{u\alpha}$, $U_{u\beta}$ represent the maximum amplitudes of the downgoing and the upgoing "P" and "S" waves respectively.

P, Q, R, S provide the plane wave characteristics as follows:

$$P = kr_\alpha z$$

$$Q = kr_\beta z$$

$$R = i (wt - ik_\alpha l_\alpha x)$$

$$S = i (wt - ik_\beta l_\beta x)$$

$i\gamma_\alpha, i\gamma_\beta$ are the ratios of vertical and horizontal amplitudes for P and S waves respectively as can be derived from equations B.10.

For waves of type i:

$$\gamma_i = \frac{W_{di}}{U_{di}} = \frac{c_{11} + c_{44} r_i^2 - \rho c^2}{- r_i (c_{13} + c_{44})} = \frac{r_i (c_{13} + c_{44})}{- \{ c_{44} + c_{33} r_i^2 - \rho c^2 \}}$$

The following substitutions are necessary to convey the solution into a more useful form:

$$U_1 = U_{u\alpha} - U_{d\alpha}$$

$$U_2 = U_{u\alpha} + U_{d\alpha}$$

$$U_3 = U_{u\beta} - U_{d\beta}$$

$$U_4 = U_{u\beta} + U_{d\beta} \qquad \text{B.20}$$

Since the position on the surface is arbitrary for plane waves, x can be set to zero. The quantity measured is not displacement but particle velocity, so the derivative of equation B.19 yields

$$\frac{\dot{u}}{c} = ik \{ U_2 \cos P + iU_1 \sin P + U_4 \cos Q + iU_3 \sin Q \}$$

$$\frac{\dot{w}}{c} = ik \{ - U_2\gamma_\alpha \sin P + iU_1\gamma_\alpha \cos P - U_4\gamma_\beta \sin Q + iU_3\gamma_\beta \cos Q \} \qquad \text{B.21}$$

Combining equations B.19, B.20, and B.5 leads to stress relationships as follows:

$$P_{zz} = ik \{ iX_\alpha U_2 \cos P - X_\alpha U_1 \sin P + iX_\beta U_4 \cos Q - X_\beta U_3 \sin Q \}$$

$$P_{zx} = ik \{ iY_\alpha U_2 \sin P + Y_\alpha U_1 \cos P + iY_\beta U_4 \sin Q + Y_\beta U_3 \cos Q \}$$

where $X_\alpha = c_{33}\gamma_\alpha r_\alpha + ic_{13}$

$$X_\beta = c_{33}\gamma_\beta r_\beta + ic_{13}$$

$$Y_\alpha = c_{44}(r_\alpha - i\gamma_\alpha)$$

$$Y_\beta = c_{44}(r_\beta - i\gamma_\beta)$$

X_α, X_β are purely imaginary while Y_α, Y_β are real. B.22

Equations B.21 and B.22 can be expressed in matrix form for any layer m.

$$\bar{V}_m = \begin{vmatrix} \frac{\dot{u}_m}{c} \\ \frac{\dot{w}_m}{c} \\ P_{zzm} \\ P_{zxm} \end{vmatrix} = ikD_m \begin{vmatrix} U_{2m} \\ U_{1m} \\ U_{4m} \\ U_{3m} \end{vmatrix} = ikD_m \bar{U}_m \qquad \text{B.23}$$

where $\bar{U}_m$ is the amplitude vector, and $\bar{V}_m$ is the particle velocity and stress vector.

$$D_m = \begin{vmatrix} \cos P_m & i \sin P_m & \cos Q_m & i \sin Q_m \\ -\gamma_{\alpha m} \sin P_m & i\gamma_{\alpha m} \cos P_m & -\gamma_\beta \sin Q_m & i\gamma_{\beta m} \cos Q_m \\ iX_{\alpha m} \cos P_m & -X_{\alpha m} \sin P_m & iX_{\beta m} \cos Q_m & -X_{\beta m} \sin Q_m \\ iY_{\alpha m} \sin P_m & Y_{\alpha m} \cos P_m & iY_\beta \sin Q_m & Y_\beta \cos Q_m \end{vmatrix}$$

At the top of the layer, z = 0, and to preserve continuity of displacement and stress across the interface, the following relation must be true.

$$\bar{V}_{m-1} = ikE_m \bar{U}_m$$

where $E_m = D_m$ at $z = 0$, or

$$E_m = \begin{vmatrix} 1 & 0 & 1 & 0 \\ 0 & i\gamma_{\alpha m} & 0 & i\gamma_{\beta m} \\ iX_{\alpha m} & 0 & iX_{\beta m} & 0 \\ 0 & Y_{\alpha m} & 0 & Y_{\beta m} \end{vmatrix} \qquad \text{B.24}$$

Restating B.23 and B.24, one has

$$\bar{V}_m = ikD_m\bar{U}_m \qquad \text{(B.23)}$$

$$\bar{V}_{m-1} = ikE_m\bar{U}_m \qquad \text{(B.24)}$$

therefore

$$\bar{U}_m = \frac{E_m^{-1}\bar{V}_{m-1}}{ik}$$

and

$$\bar{V}_m = D_m E_m^{-1}\bar{V}_{m-1} \qquad \text{B.25}$$

where

$$E_m^{-1} = \begin{vmatrix} -A_m X_{\beta m} & 0 & -iA_m & 0 \\ 0 & -iB_m Y_{\beta m} & 0 & -B_m \gamma_{\beta m} \\ A_m X_{\alpha m} & 0 & iA_m & 0 \\ 0 & iB_m Y_{\alpha m} & 0 & B_m \gamma_{\alpha m} \end{vmatrix}$$

where $$A_m = \frac{1}{X_{\alpha m} - X_{\beta m}}$$

$$B_m = \frac{1}{\gamma_{\alpha m} Y_{\beta m} - \gamma_{\beta m} Y_{\alpha m}}$$

A_m is purely imaginary while B_m is real.

Let $$a_{m-1} = D_{m-1} E_{m-1}^{-1}. \qquad \text{B.26}$$

Then B.21 becomes for the (m-1) layer:

$$\bar{V}_{m-1} = a_{m-1} \bar{V}_{m-2} \qquad \text{B.27}$$

Repeatedly substituting in equation B.20, a recurrent relationship can be established starting with the bottom layer n until the surface is reached:

$$\bar{U}_n = \frac{E_n^{-1}}{ik} a_{n-1}, a_{n-2} \ldots a, \bar{V}_0 \qquad \text{B.28}$$

$$J = E_n^{-1} a_{n-1} a_{n-2} \cdots a, \qquad \text{B.29}$$

Using substitutions B.20, the boundary condition that stress must vanish at the free surface, and assuming an incident P wave at the base of layer n-1

$$U_{u\alpha n} = 1 \quad \text{and} \quad U_{u\beta n} = 0 \qquad \text{B.30}$$

$$\begin{vmatrix} 1 + U_{d\alpha n} \\ 1 - U_{d\alpha n} \\ - U_{d\beta n} \\ U_{d\beta n} \end{vmatrix} = \frac{J}{ik} \begin{vmatrix} \frac{\dot{u}_0}{c} \\ \frac{\dot{w}_0}{c} \\ 0 \\ 0 \end{vmatrix} \qquad \text{B.31}$$

Solving these equations for the normalized particle velocities, one arrives at the crustal transfer functions.

$$U_p = \frac{\dot{u}_0}{c} = - \frac{2ik}{D} (J_{32} + J_{42}) = \text{horizontal transfer function}$$

$$W_p = \frac{\dot{w}_0}{c} = \frac{-2ik}{D} (J_{31} + J_{41}) = \text{vertical transfer function} \qquad \text{B.32}$$

where D is the determinant of coefficients from equations B.31

$$D = -\frac{1}{k^2} (J_{12} + J_{22}) (J_{31} + J_{41}) + \frac{1}{k^2} (J_{11} + J_{21}) (J_{32} + J_{42})$$

The ratio of the moduli of the above complex expressions gives the theoretical P-coda spectral ratio (R) for any assumed crustal model. It can be shown that elements J_{32} and J_{41} are purely imaginary whereas J_{31} and J_{42} are real.

$$R = \frac{|W_p|}{|U_p|} = \left| \frac{W_p}{U_p} \right| = \left| \frac{J_{31} + J_{41}}{J_{32} + J_{42}} \right| = \left[\frac{J_{31}^2 + J_{41}^{*2}}{J_{32}^{*2} + J_{42}^2} \right]^{1/2}$$

where $iJ_{41}^{*} = J_{32}$ B.33

The spectral ratio can thus be seen to be dependent only on the matrix J, a function of the layer parameters, frequency, and angle of incidence of the wave.

APPENDIX C

P-CODA PLOTS OF THE FOUR FALL 1969 ALEUTIAN EVENTS

AS RECORDED AT STATIONS OBS, VNG, AND OSC

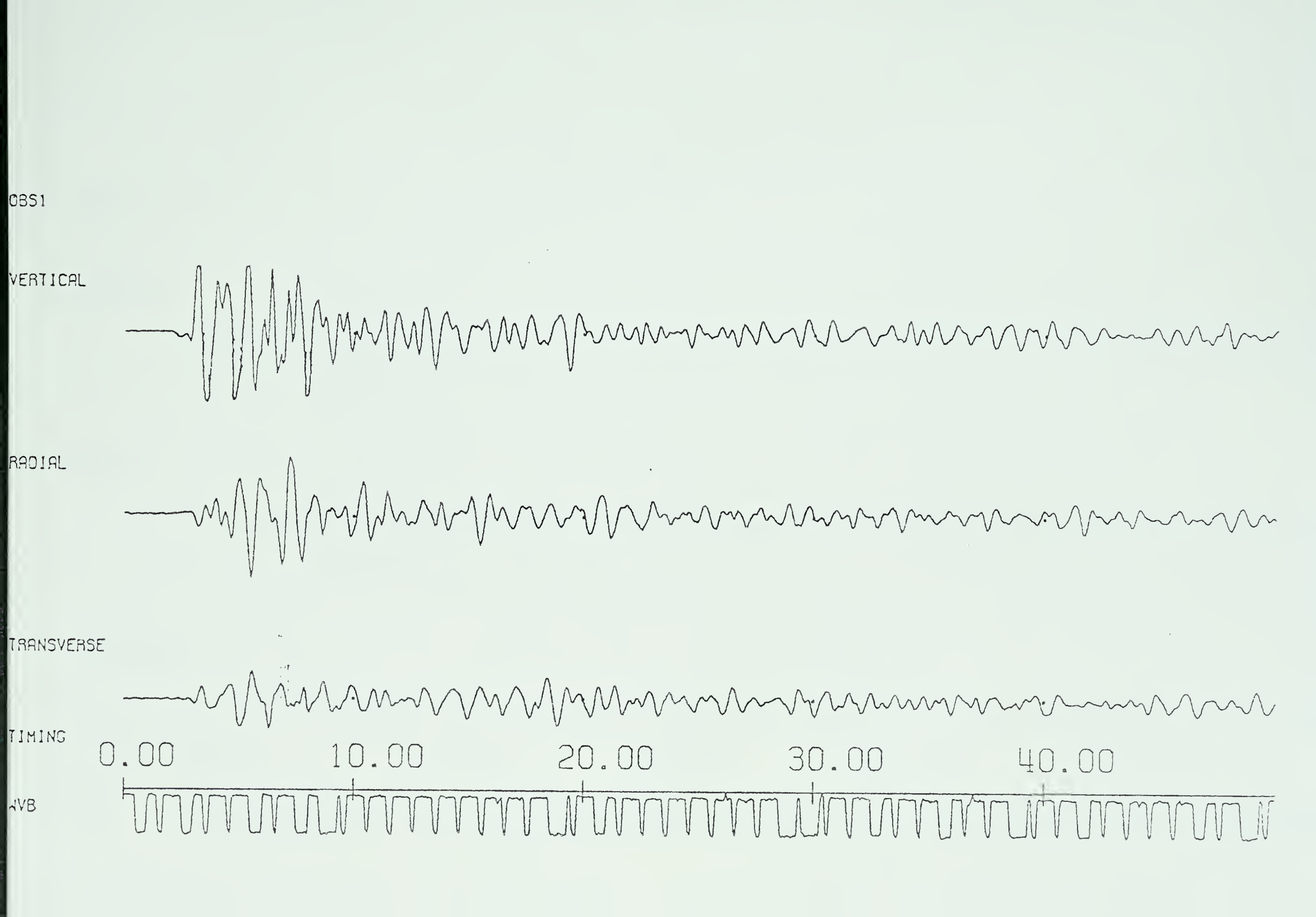
OBS1
VERTICAL
RADIAL
TRANSVERSE
TIMING
0.00
10.00
20.00
30.00
40.00
NVB

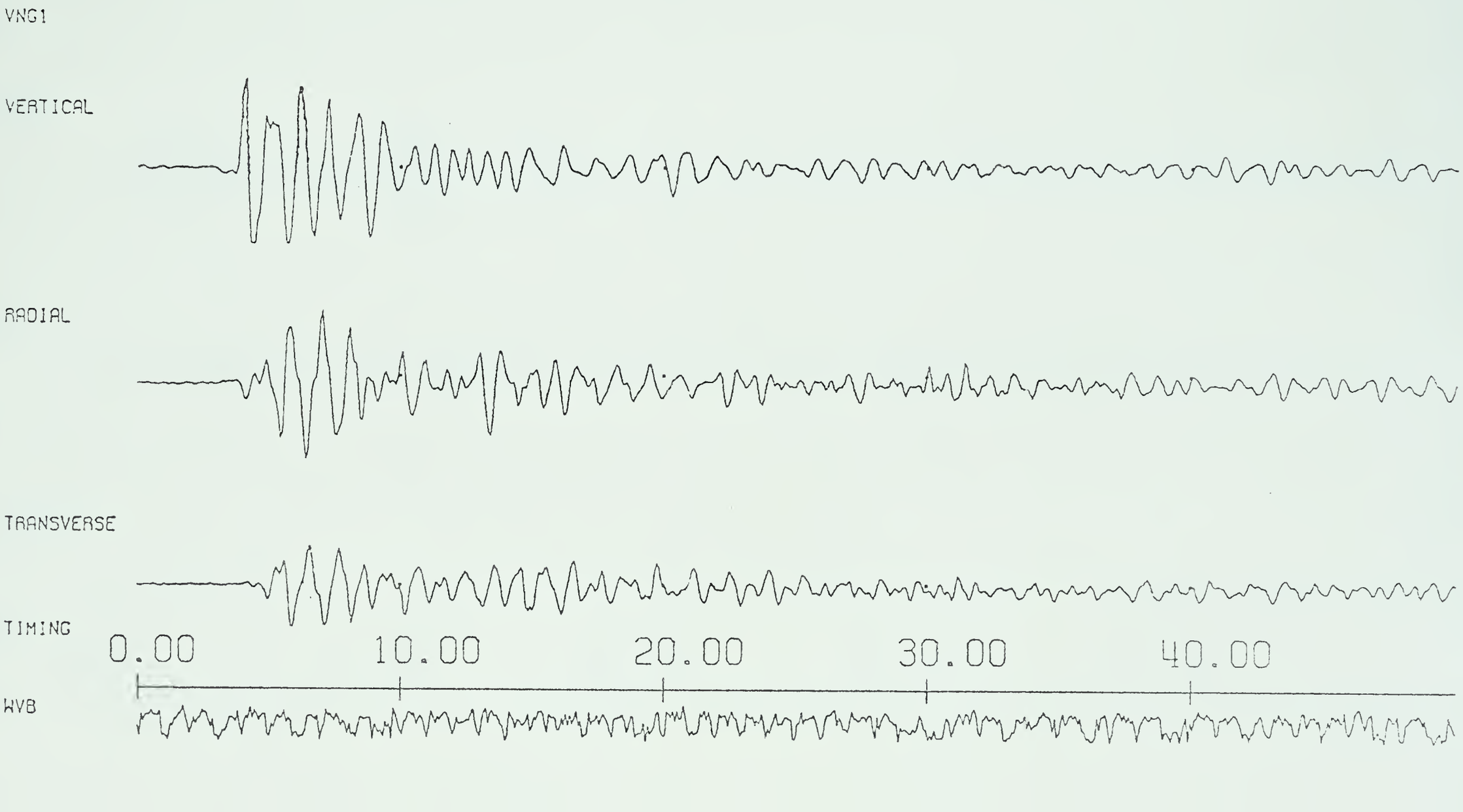
VNG1
VERTICAL
RADIAL
TRANSVERSE
TIMING
0.00
10.00
20.00
30.00
40.00
WVB

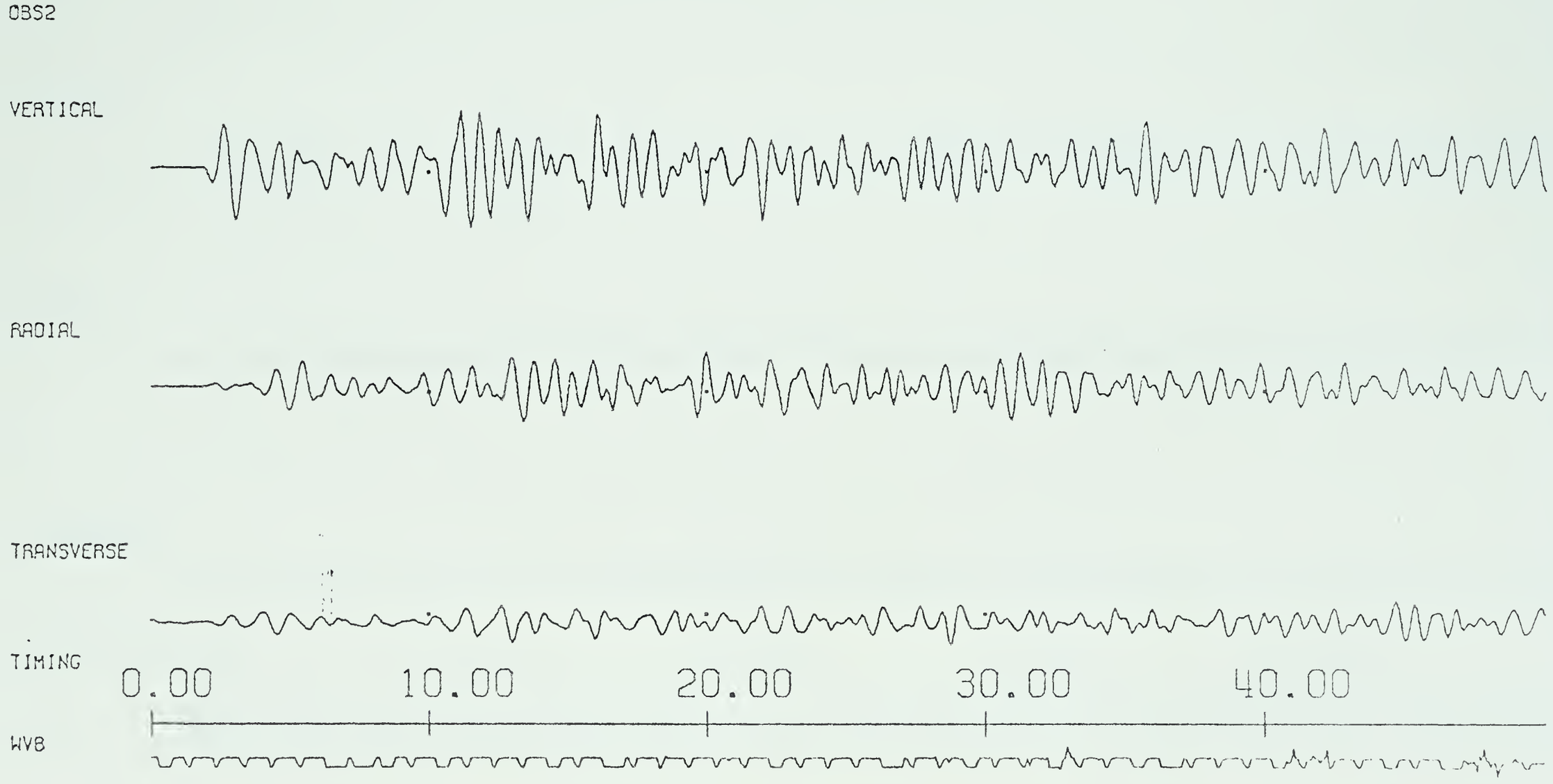
OBS2
VERTICAL
RADIAL
TRANSVERSE
TIMING
0.00
10.00
20.00
30.00
40.00
WVB

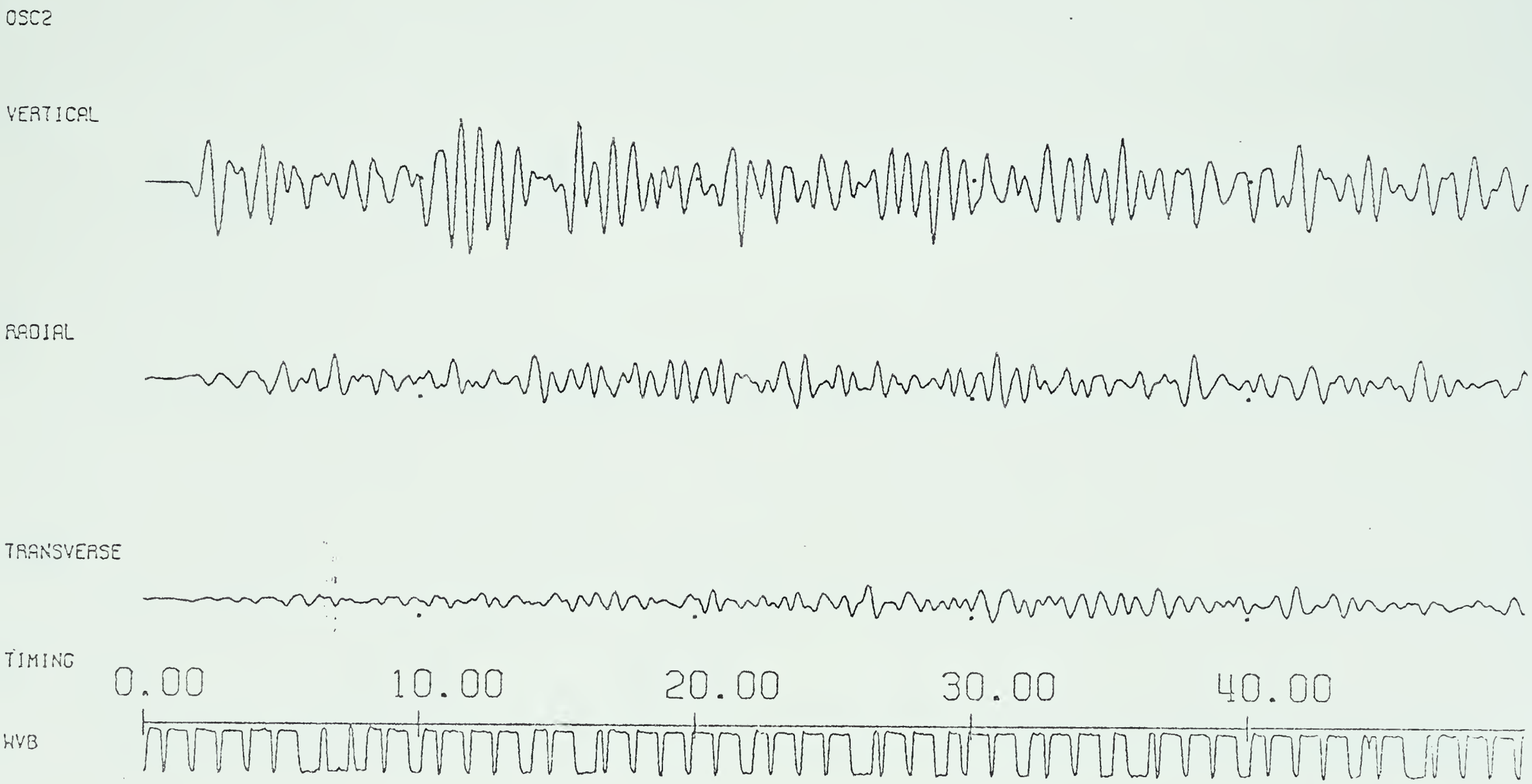
OSC2
VERTICAL
RADIAL
TRANSVERSE
TIMING
0.00
10.00
20.00
30.00
40.00
HVB

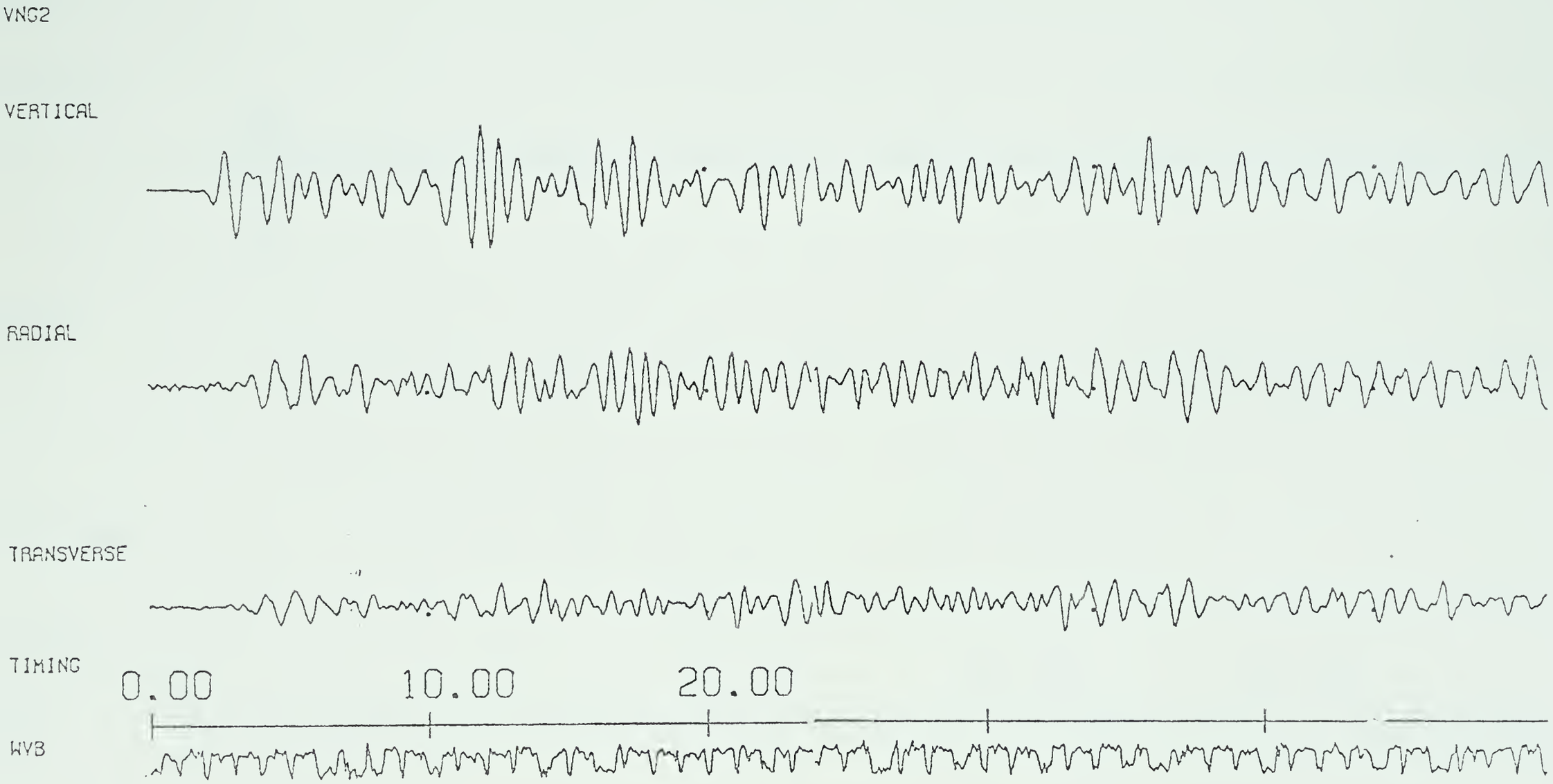
VNG2
VERTICAL
RADIAL
TRANSVERSE
TIMING
0.00
10.00
20.00
WVB

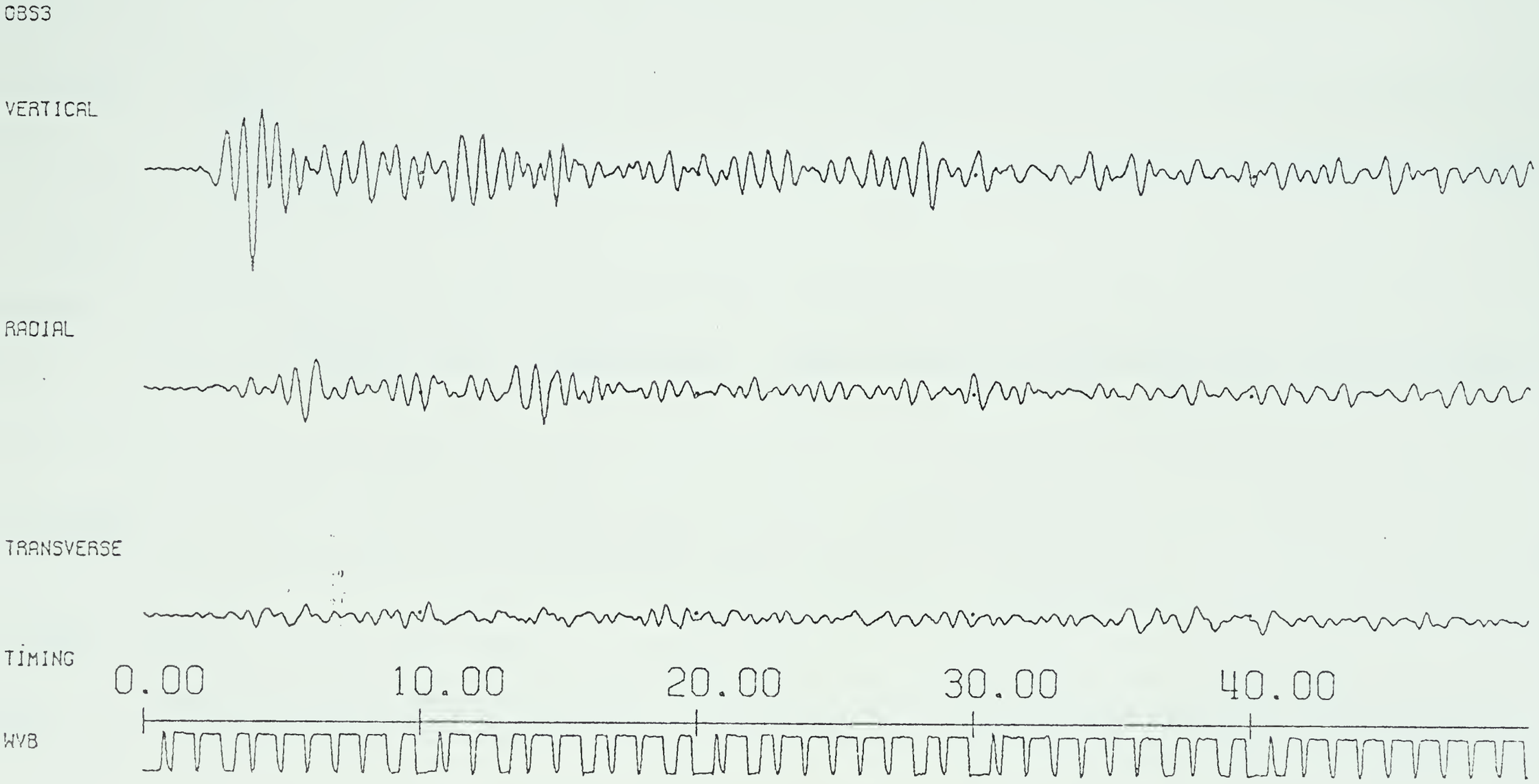
OBS3
VERTICAL
RADIAL
TRANSVERSE
TIMING
0.00
10.00
20.00
30.00
40.00
WVB

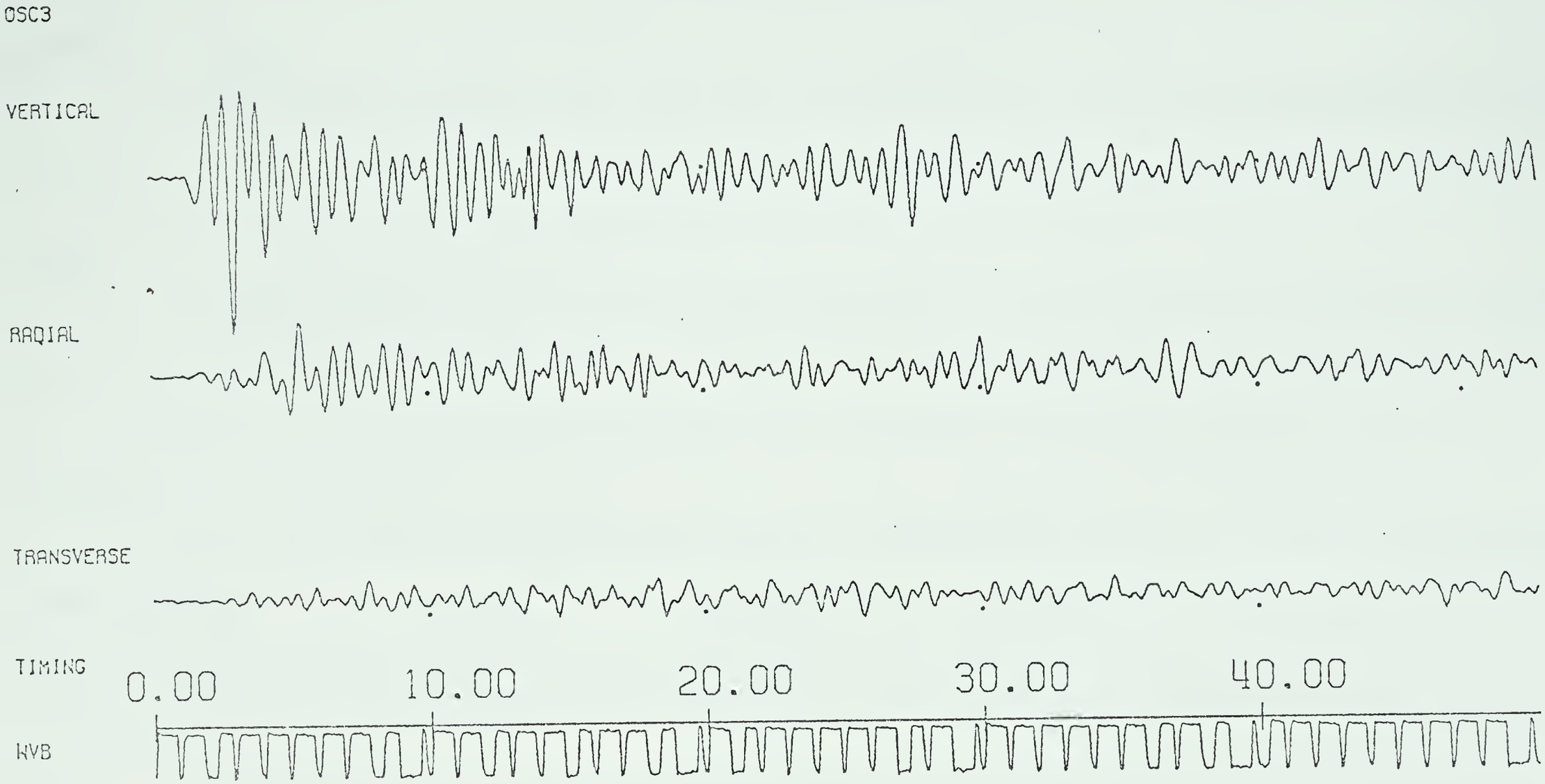
OSC3
VERTICAL
RADIAL
TRANSVERSE
TIMING
0.00
10.00
20.00
30.00
40.00
NVB

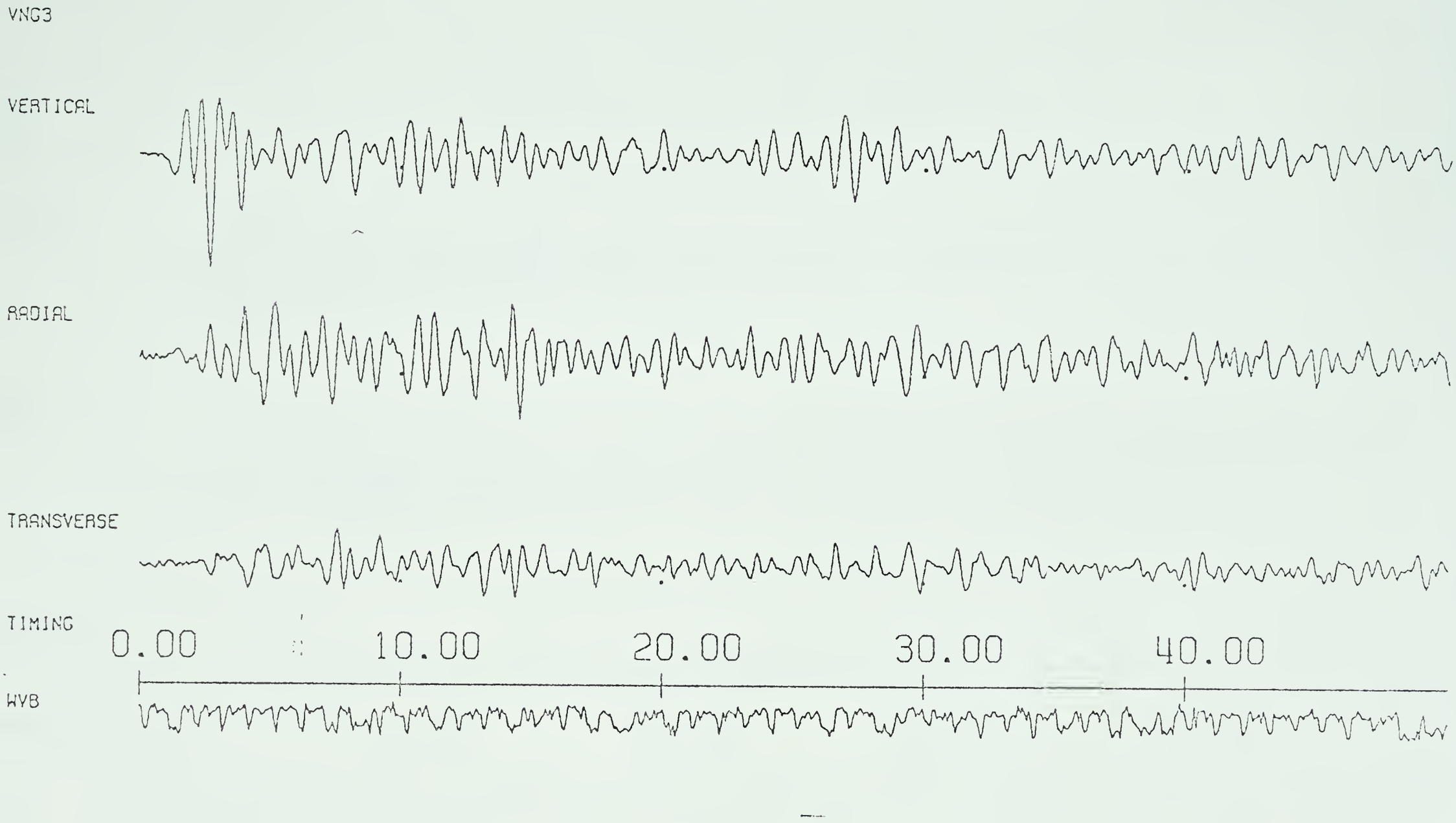
VNG3
VERTICAL
RADIAL
TRANSVERSE
TIMING
0.00
10.00
20.00
30.00
40.00
WVB

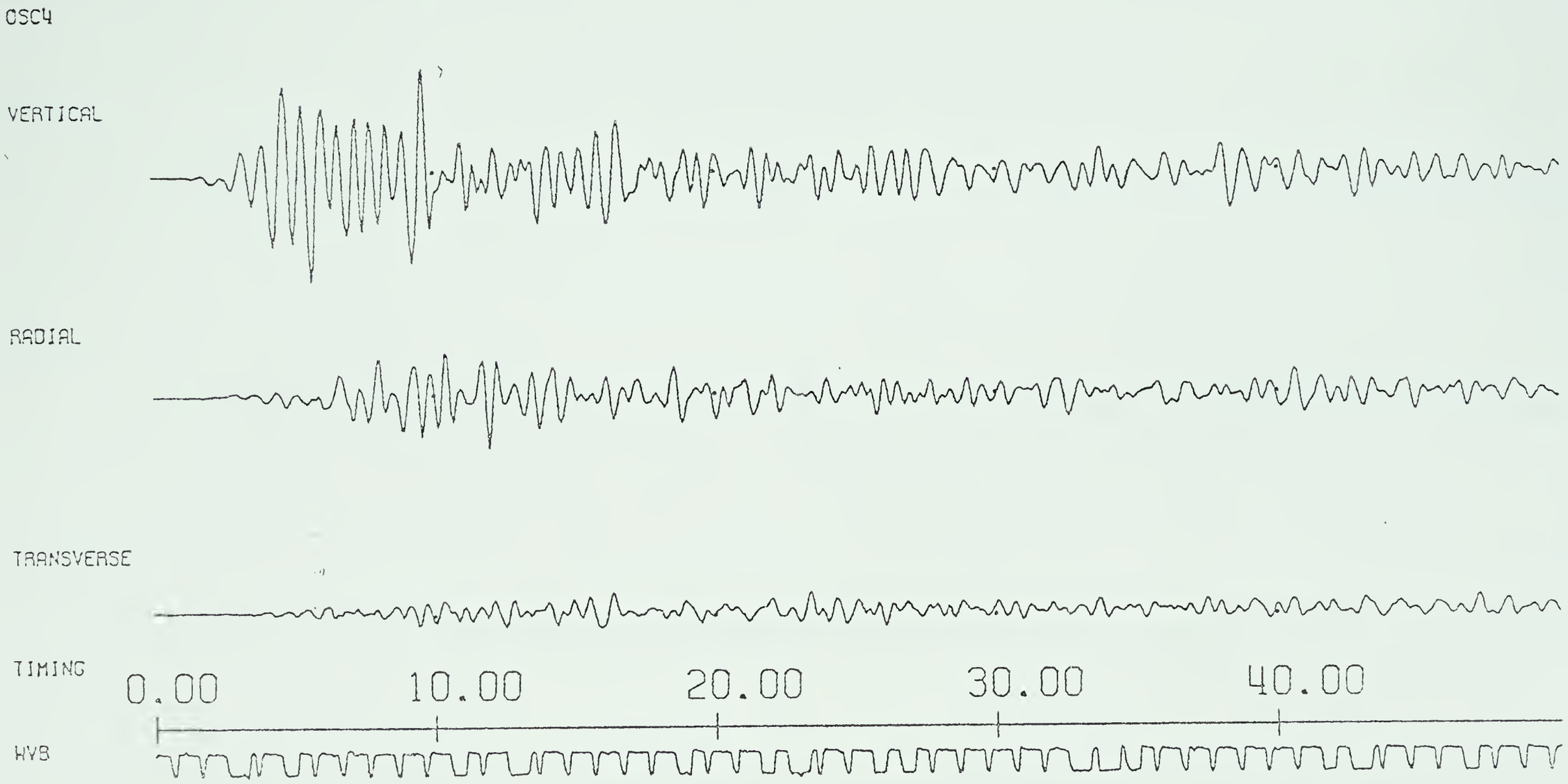
OSC4
VERTICAL
RADIAL
TRANSVERSE
TIMING
0.00
10.00
20.00
30.00
40.00
HVB

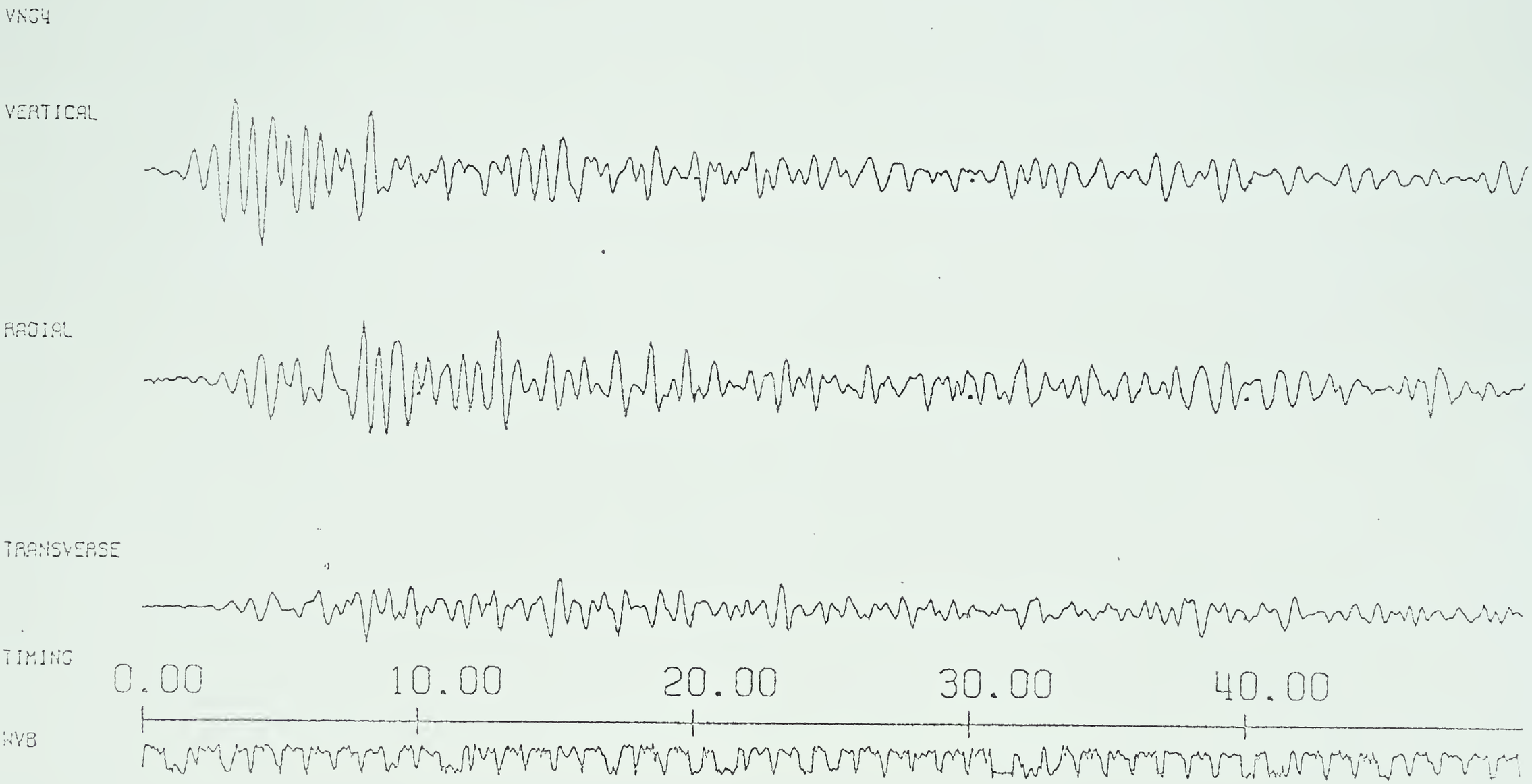
VNG4
VERTICAL
RADIAL
TRANSVERSE
TIMING
0.00
10.00
20.00
30.00
40.00
NVB